

Stony Brook University



OFFICIAL COPY

The official electronic file of this thesis or dissertation is maintained by the University Libraries on behalf of The Graduate School at Stony Brook University.

© All Rights Reserved by Author.

Photonic and Phononic Engineered Materials

A Dissertation Presented

by

Samrat G. Chawda

to

The Graduate School

in Partial Fulfillment of the

Requirements

for the Degree of

Doctor of Philosophy

in

Materials Science and Engineering

Stony Brook University

August 2009

Copyright by
Samrat G. Chawda
2009

Stony Brook University

The Graduate School

Samrat G. Chawda

We, the dissertation committee for the above candidate for the
PHD in Materials Science and Engineering, hereby recommend acceptance of this
dissertation.

Dr. Charles Fortmann – Dissertation Advisor
Professor, Department of Materials Science and Engineering

Dr. Gary Halada
Professor, Department of Materials Science and Engineering

Dr. Jon Sokolov
Professor, Department of Materials Science and Engineering

Dr. Hazem Tawfik – Chair person of Defense
Distinguished Professor, Department of Mechanical Engineering Technology, SUNY
Farmingdale

This dissertation is accepted by the Graduate School

Lawrence Martin
Dean of the Graduate School

Abstract of the Dissertation

Photonic and Phononic Engineered Materials

by

Samrat G. Chawda

Doctor of Philosophy

in

Materials Science and Engineering

Stony Brook University

2009

Amorphous silicon based integrated photonics technology has been a developing field over the last few years. Research to develop several types of photonic devices is ongoing. One of the important materials in this field of research is hydrogenated amorphous silicon (a-Si:H). This material, owing to its easy preparation (hot-wire chemical vapor deposition), large amount of hydrogen intake (for refractive index changes), and ease of use for photolithographic and etching techniques is being used for this work. Wave guides have been prepared and demonstrated, and structures were characterized using Raman spectroscopy.

As this field continues to evolve, the prospect of phonons, generated in a-Si:H, to convey information from one location to another is investigated. Samples with different thickness and different concentrations of hydrogen were investigated using Raman spectroscopy in conjunction with a bias light. Results show that phonon

transport in amorphous silicon thin films is feasible. Phonon lifetime and its diffusion are also studied related to the film thickness and its hydrogen content. The result leads us to a new field of phonon engineering and phononic engineered materials.

The design considerations for a spectra modifying, light scattering for one phononic device application is the spectral modification for solar cells were investigated. Efficient commercially available phosphors absorb one near Infrared (IR) photon and one near Ultraviolet (UV) photon and emit one photon in the visible spectrum. There by such phosphors offer the possibility to convert two poorly utilized portions of solar spectrum to photons that are converted to electrical energy with high quantum efficiency in solar cells. Here the light scattering and spectral conversion of silicon nano particles is explored. Silicon nano-particles offer relatively low absorption for below gap light and the potential to convert UV to visible via luminescence and IR to visible via multiple Raman shifts. Furthermore, it is found that silicon nano-particles in a high refractive index media effectively scatter light.

To Sri. Ghanshyam Chawda and Smt. Bharati Chawda who are a constant source of support, encouragement and who have taught me a few priceless treasures of sincerity, faith, hope and love. For Geetanjali Chawda for having the patience to put up with me now and the rest of my life...

For Ritesh 'DON' Chawda for all the beautiful memories...

Table of Contents

| | |
|--|-----|
| LIST OF FIGURES..... | vii |
| LIST OF TABLES | ix |
| ACKNOWLEDGEMENTS..... | x |
| PUBLICATIONS..... | xi |
| 1. INTRODUCTION: MOTIVATION BEHIND THIS WORK..... | 1 |
| 2. AMORPHOUS SILICON | 6 |
| 2.1. Hydrogenated Amorphous Silicon | 7 |
| 2.1.1. Role of Hydrogen..... | 7 |
| 2.1.2. Refractive Index and Hydrogen..... | 8 |
| 2.1.3. Amorphous Silicon Optical Band Gap and Hydrogen..... | 10 |
| 2.1.4. Wave Guides in a:Si-H: Experiments and Techniques..... | 11 |
| 2.1.5. Light Induced Changes in a:Si-H..... | 14 |
| 3. PHONONIC HYDROGENATED AMORPHOUS SILICON..... | 16 |
| 3.1. Introduction to Phonons..... | 16 |
| 3.2. Phonon Gap and Hydrogen Dependence..... | 18 |
| 3.3. Controlling and Utilizing Phonon Energy | 23 |
| 4. a:Si BASED SOLAR CELLS: SPECTRAL MODIFICATIONS..... | 28 |
| 4.1. Solar Spectrum | 28 |
| 4.2. a:Si based solar cells..... | 33 |
| 4.2.1. a:Si solar cells and multi-junction approach..... | 34 |
| 4.3. Silicon nanoparticles and solar cells..... | 35 |
| 4.3.1. Photo-luminescence of silicon nanoparticles..... | 36 |
| 4.3.2. Reasons for photo-luminescence of silicon nanoparticles | 37 |
| 4.3.3. Raman spectra of silicon nanoparticles..... | 39 |
| 5. EXPERIMENTS, RESULTS AND DISCUSSION | 42 |
| 5.1. Theoretical Considerations | 43 |
| 5.2. Light diffusivity in thin-film semiconductors | 44 |
| 5.3. Experiments and results..... | 51 |
| 5.4. Conclusions | 53 |
| BIBLIOGRAPHY | 55 |

LIST OF FIGURES

| | |
|--|----|
| Figure-2.1 The amorphous silicon refractive index Vs. Hydrogen content for 633 nm (dashed line) and 2.5 micron (dots and solid line) based on the data of [15] and [16]..... | 9 |
| Figure-2.2 Use of photolithography and hydrogen implants to create a refractive index gradient [24]. | 11 |
| Figure-2.3 Steps to prepare hydrogen implant patterned hydrogenated amorphous silicon films. | 13 |
| Figure-2.4 Illuminated a-Si:H film. | 14 |
| Figure-3.1 Raman scattering of a photon with emission or absorption of a phonon. | 17 |
| Figure-3.2 E-k diagram. a- photon absorption for direct band gap semiconductor. b- photon absorption along with phonon absorption in indirect band gap semiconductor. c- photon absorption along with phonon emission in indirect band gap semiconductor. | 20 |
| Figure-3.3 Changes in crystalline silicon band diagram to explain the hydrogen dependence. | 22 |
| Figure-3.4 Liquid nitrogen cooled sample holder. | 24 |
| Figure-3.5 Raman spectra for samples with 2-3% hydrogen. | 25 |
| Figure-3.6 Using an amorphous silicon bridge phonons induce an anti-Stokes shift in the first beam whenever a second beam is present in waveguide 2. The magnitude of the shift is proportional to the magnitude of each of the beams and the shift itself is a function of the amorphous material used for the bridge..... | 26 |
| Figure-4.2 Solar intensity varying with the wavelength | 30 |
| Figure-4.3 The quantum efficiency of a silicon solar cell | 31 |
| Figure-4.4 Light absorption and transmission of different photovoltaic material | 32 |

| | |
|---|----|
| Figure-5.1 Key elements of a Raman-based photon energy up-converting nano-particle silicon dispersed in a TiO ₂ matrix applied to the back of a solar cell..... | 44 |
| Figure-5.2 Light diffusion in a thin film semiconductor. | 45 |
| Figure-5.3 Relation between the current flux for different bandgap semiconductors. | 50 |
| Figure-5.4 Optical micrograph of 50nm silicon nanoparticles under white light (a), collimated laser diode illumination (b) and broad spectrum 254 nm illumination. | 52 |
| Figure-5.5 Raman shift comparison for different sizes silicon nanoparticle powder and C-silicon. | 53 |

LIST OF TABLES

| | |
|--|----|
| Table 3.1 Calculated area under 490cm^{-1} Raman Peak..... | 25 |
| Table 4.1 Current amorphous and thin-film approaches | 34 |

ACKNOWLEDGEMENTS

Knowledge, guidance, encouragement and support are important ingredients that make up a graduate student's life. My years at Stony Brook would not have been the same without these.

I have been bought up by the saying 'For a student a teacher is his God'. I would like to express my appreciation to my teacher and mentor Professor Charles Fortmann, for providing me this opportunity, without his knowledge, support, enthusiasm, faith and patience this work would not have been possible. I'm proud to be associated with him.

I would like to thank to Professor Gary Halada and Professor Clive Clayton for their guidance over the past few years and providing me a space in their lab. Their inputs, guidance, support have always been positive and encouraging. Furthermore, I would like to thank Professor Richard Gambino, Dr. Jim Quinn and Professor Alexander Orlov for graciously providing me the access to their laboratory facilities. Much appreciation and thanks to Professor Jon Sokolov and Professor Hazem Tawfik for having time to be on my committee.

Thanks to all my friends, colleagues for sharing their valuable knowledge and helping me in all possible ways. Special thanks to Prashant, Jose, Kasia, Anand, Gajendra, Pranav, Ashish, Supradeep, Mike's, Don, Anne, Saskya, Chris's, Joe, Lory, Debby, Lynn and Lester for all the good 'spirits'. Finally I take this opportunity to thank God for His generous providence.

PUBLICATIONS

Following publications have been the outcome of this research.

- [1] C. M. Fortmann, **S. G. Chawda** and Rose Ping Lee, “Nano-Particle Silicon for Raman-based Spectral Up-conversion”, International Conference of Amorphous and Non-crystalline Materials, 2009, Paper Submitted.
- [2] **S. G. Chawda**, J. A. Mawyin, G. P. Halada, C.M. Fortmann, “Phononic Engineered Materials and Devices”, Journal of Non-crystalline Solids 354, 2548-2551, (2008).
- [2] J. A. Mawyin, **S. G. Chawda**, G. P. Halada, C. R. Clayton, C. M. Fortmann, “Substrate Engineering for High Efficiency Thin Film Solar Cells”, Journal of Non-crystalline Solids 354 2492-2494, (2008).
- [3] **S. G. Chawda**, J. A. Mawyin, A. H. Mahan, C. M. Fortmann and G. P. Halada, “Phononic Amorphous Silicon: Theory, Materials and Devices”, Mater. Res. Soc. Symp. Proc. 910, Matl. Res. Soc. (2006).
- [4] G. P. Halada, **S. G. Chawda**, J. A. Mawyin, R. J. Tonucci, A. H. Mahan, C. M. Fortmann, “Advances in Amorphous Silicon Integrated Photonics Science and Technology”, Mater. Res. Soc. Symp. Proc. 862, Matl. Res. Soc. (2005).

INTRODUCTION

Motivation behind this work

'Light' is the fastest information conveying entity; Revolutions in fiber optics and laser technology have enabled long distance light based information conveyance to become the norm in the last decade or so. This revolution was in-turn enabled by a host of material advances in glass fibers and Gallium Arsenide-based opto-electronics devices (including lasers).

Crystal Silicon and silicon material research enabled a similar revolution in integrated electronic devices decades earlier starting in the 1960's. More recently thin film amorphous silicon materials have fueled a multi-billion dollar revolution in flat panel display technologies. It is safe to say that the advances of the latter half of the twentieth century were based upon a silicon revolution. However, the role of silicon in light-based information conveyance is just now emerging. Perhaps like no technology in human history silicon enters the opto-electronic arena with a vast and detailed material understanding.

Silicon as a semiconductor material has made its way into the lifestyle of people in an immense, all most indescribable manner; medical devices, computers, almost all of the solar cells used to power satellites and 95% of the terrestrial solar electric power generated, automated engine and system controls in cars and aircraft, cameras, games and many more applications to come. Presently most of the silicon applications are electronic,

use electrical signals. Greater reliance on the optical properties of silicon is emerging as one of the cornerstones of next generation of silicon-based technologies particularly for information conveyance.

Presently optical-based information conveyance requires conversion of electrical signals into optical signals for long distance conveyance and the conversion back into electrical signal for procession. Present technology employs a number of semiconductor platforms to perform these various tasks. For example, Gallium-Arsenide materials are often used for converting electrical signals and energy into light. However, more of these processes are being formed by silicon in ways that lend themselves to monolithic integration into a single silicon chip. This evolution will both reduce costs and increase device speed and performance.

Owing to its desirable optical properties, silicon is an important, as well as ideal material for photonic-semiconductors. Silicon is transparent to infrared wavelengths [1], since; present era information conveyance is based on IR and near IR light transmission on glass-based fiber optic cables. Researchers from Intel recently introduced an all silicon-laser using a physical property called the Raman Effect related to the interaction of crystal lattice waves (phonons) with light. This can lead us to applications such as optical amplifiers, silicon-lasers and new kind of lossless optical devices [1]. This work focuses on the prospect of utilizing these lattices waves (phonons) as the basis for a new generation of devices on engineered phonon-light-electrical interactions.

In recent developments, researchers from Cornell University have created a broadband light amplifier on a silicon chip [2]. This shows us that the combination of photonics and electronics can be easily made on the same chip. Research on silicon nano-

crystals received a boost by reported observation of net optical gain in SiO₂ waveguides doped with silicon nano-crystals [3]. By using well established techniques of photolithography and etching of silicon based materials, researchers have been able to pattern tiny circuits of materials with different refractive indices [4]. An all-silicon optical modulator with modulation bandwidth exceeding 1GHz has also been demonstrated [5] which further tells us that monolithic integration of the silicon modulator with advanced electronics on a single silicon substrate is possible. Ongoing research shows it has become easy to teach Silicon new tricks.

Silicon has long been the ideal material for electronics, but it is only relatively recently that it has been considered as a material for photonics [6]. Photonic devices control light propagation through refractive index engineering. Amorphous silicon can be one of the most ideal materials for engineering photonic and integrated optical circuits. Amorphous silicon based material has an advantage because its structure can accommodate large quantities of impurities (hydrogen in this case) (reference Fortmann SPIE 1999).

Amorphous silicon is an ideal material matrix for photonics and phononics applications, considering the fact that the refractive index can be significantly changed by hydrogen implantation. The amount of this impurity (or hydrogen implantation) can be used to define photonic structure such as waveguides. Along with the engineering of waveguides and related structures using amorphous silicon-based thin films for the purpose of shaping and controlling flow of light, this work will also introduce the potential of using phonons to convey information. The field of phononic-engineered amorphous silicon is explored, specifically the construction of

devices and waveguide for information conveyance and manipulation via phonons. Amorphous silicon, owing to the inherent scattering structures and localization (of some phonon bands), has an anomalously large phonon lifetime [7]. The indirect optical band gap of amorphous silicon provides the physical basis for the transduction of phonon and optical energies [8]. Experimental methods to probe phonon spectra and its transport and the prospect of a fully integrated phononic, photonic and electronic amorphous silicon technology are described.

Silicon being highly abundant in the earth's crust and due to its band structure, it is an ideal material for photovoltaics. Crystalline silicon based photovoltaics make up to ~95% of the photovoltaic sales worldwide [45]. Thin film amorphous silicon based photovoltaics are being researched in the photovoltaics research/markets, as they provide for much higher efficiency's in a solar cell. The vista provided by over thirty years of amorphous silicon-based solar cell advancement provides a clear view to development of substantial solar electric generation. Amorphous silicon solar cells have demonstrated impressive performance and stability in the multi-junction approach.

This work also examines inexpensive layers that can be applied to regular solar cell to: increase the acceptance angle of solar irradiation, provide strong scattering and reflection of light back into a solar cell for multiple passes, and through phonon related process broaden the solar spectrum to facilitate higher efficiency conversion into electrical power. Also, the photoluminescence properties of silicon nano-particles have been explored. These nano-particles are used as a phosphor spectral modification layer applied in front of a solar cell to facilitate favorable spectral conversion of light for

higher efficiency.

One of the important properties of Silicon nano-particles is it offers the prospect of IR up-conversion through Raman (anti-Stokes) scattering. Silicon in general is known to have an exceptionally large Raman shift. Silicon based Raman laser has been demonstrated [1]. Silicon nano particle-based Raman up and down conversion offers the best prospect for solar cell back surface applications (since, the strongly absorbed visible light is removed prior to encountering the silicon nano-particles parasitic light absorption by the particles is reduced).

CHAPTER 2

Amorphous Silicon

Amorphous silicon (a-Si) is non-crystalline form of silicon. Silicon is normally tetrahedrally bonded to four neighboring silicon atoms, which is also true in the case of a-Si, however, in this case, the long-range order is not present, and the atoms form a continuous random network. The short range order is directly responsible for observable semiconductor properties such as optical absorption edges and activated electrical conductivities [9]. Amorphous silicon can have large concentrations of dangling bonds which generally makes the material hard to work with. The electron energy levels of a dangling bond lie between the valence and conduction states of fully paired, bonded electrons. These states in the gap contribute to the optical absorption and electrical conduction processes, masking the measurement of the energy gap in either process. In other words the dangling bonds produce states inside the energy gap that can reduce the mobility of the electrons (carrier trap), and they also act as nonradiative recombination centers that decrease the carrier life time which results in a very small amount of photoconductivity (or photoluminescence) in a-Si.

These above mentioned defects are highly undesirable for any devices. However, hydrogen passivates these dangling bonds in turn eliminating the carrier traps and nonradiative recombination centers.

2.1 Hydrogenated Amorphous Silicon

Hydrogenated amorphous silicon (a-Si:H) was first prepared in late 1960s by Chittick and coworkers from a glow discharge in silane (SiH_4) [10]. This technique is the same as is used currently along with the addition of new and better design for deposition systems. The early experiments (Chittick *et al.* 1969, Chittick and Sterling 1985) on this material showed the lack of conduction in defect states and increased conduction due to impurities. However, the important optical properties of a-Si:H were first introduced by Spear *et al.*, showed that the material had a strong photoconductivity resulting from a very low defect density [11].

The hydrogen content range of a-Si is remarkable, unlike crystalline silicon where the hydrogen concentration is much less one atomic percent (atomic %), the solubility of hydrogen in a-Si exceeds 25% atomic percent. Hydrogen content strongly influences some of the important optical properties required for photonic engineering: the optical band gap [8, 12–14], the refractive index [15, 16], and the sub-gap absorption [17].

2.1.1 Role of Hydrogen

As explained earlier, other than passivation of dangling bonds in amorphous silicon, high concentration of hydrogen gives a much larger band gap for a-Si than that of crystalline silicon. Typically the band gap for a-Si:H is $1.7 \pm 0.2 \text{ eV}$ compared to 1.1 eV for crystalline silicon [18]. This is because Si-H bond is much stronger than the Si-Si bond, which further tells us that the average binding energy of hydrogenated

amorphous silicon is much higher than that of crystalline silicon. The energy gap scales with the binding energy, hence a larger energy gap is obtained in a-Si:H [19]. By hydrogenation, the material has a reduced density of states inside the gap which helps controlling the position of fermi level. Hence it is possible to make a-Si:H n-type or p-type at will which is not possible in non-hydrogenated amorphous silicon.

2.1.2 Refractive Index and Hydrogen

Refractive index patterning is possible through hydrogen implantation and/or in-diffusion. Beyer [20] demonstrated that hydrogen doses up to 10^{17}cm^{-2} could be implanted into amorphous silicon films. Based on the data reported by Manfredotti *et al* [15], in atomically dense amorphous silicon the relationship between refractive index for the wavelength region between 2.5 and $5\mu\text{m}$ and hydrogen content is given by Eq. 2.1:

$$\eta_{2.5-5\mu\text{m}} \approx -1.03 \times 10^{-2} C_H (\text{at.}\%) + 3.52 \text{ --- (2.1)}$$

At shorter wavelengths (623.8 nm) [16] shows the relationship between refractive index and hydrogen content grown by an expanding thermal plasma deposition technique at different substrate temperatures and growth rates, this relationship is given by Eq. 2.2:

$$\eta_{632.8\text{nm}} \approx -3.6 \times 10^{-2} C_H (\text{at.}\%) + 4.5 \text{ --- (2.2)}$$

where η is the refractive index at the specified wavelength, and C_H is the amorphous silicon hydrogen content in atomic percent. Hydrogen in amorphous silicon can be varied from 1-30 at% for long wavelength, the variation is over 15%

and at the shorter wavelength the variation is much greater (e.g., ~25% refractive index difference between 1% and 30% hydrogen content in amorphous silicon films). The experimentally determined refractive index versus hydrogen content derived from the data of [15] and [16] is given by figure 2.1. The large changes in refractive index that are associated with the hydrogen content of as-grown amorphous silicon films is shown by figure 2.1. As is clear from the figure, the refractive index can be varied by almost a factor of two in some cases. These changes demonstrate an important aspect of amorphous silicon technology, implying that the accommodation of vast amounts of hydrogen, which in turn, can be used to significantly alter the refractive index.

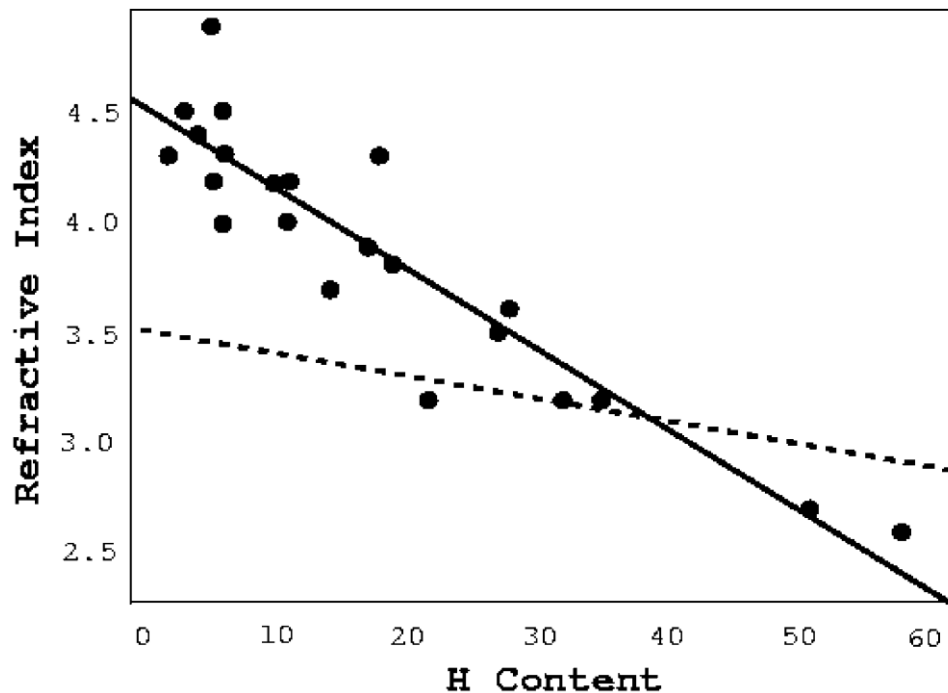


Figure 2.1: The amorphous silicon refractive index Vs. Hydrogen content for 633 nm (dashed line) and 2.5 micron (dots and solid line) based on the data of [15] and [16].

2.1.3 Amorphous Silicon Optical Band gap and Hydrogen

One of the important differences between amorphous and crystalline silicon is the amount of hydrogen that can be accommodated and the various bonding configurations hydrogen can occupy in amorphous lattice. Amorphous silicon can absorb almost 10 times more hydrogen than crystalline silicon [20]. The band gap of void free amorphous silicon is dependent on the various H-Si bonding configuration and their density [14]. In these structures the total hydrogen content, the structure factor (the ratio of the density of Si-H₂ sites to that of Si-H sites) and the Si-H site density were loosely correlate to the band gap [14]. Fortmann [8] developed an expression relating the Si-H₂ concentration to the Tauc band gap that applies to a wide range of the amorphous silicon films with band gap ranging from 1.52 to over 2.1 eV:

$$E_g (eV) = 1.47 + 0.226[C_{Si-H_2}(at.\%)]^{1/3} \quad (2.3)$$

Fortmann [8] explained the Si-H₂ dependence as seen in Eq. 2.3 by considering the Si-H₂ bonding configuration phonon scattering to be sufficiently strong so as to cause a phonon band to form. He explains the relation in terms of indirect, crystal silicon-like optical transitions with modifications resulting from site disorder in amorphous silicon. This site disorder causes the electron coherent length to become very small, which makes the portion of brillouin zone available to the amorphous silicon electron to be equivalent to a single crystal electron near the crystal zone boundary. An electron which is optically excited in this zone needs to either emit a phonon or absorb it, which is dependent on the appropriate momentum of

phonon. This occurring of phonon band gap will be further discussed in detail in the following chapter.

2.1.4 Waveguides in a:Si-H – Experiments and Techniques

A waveguide can be considered as an optical analogue for an electronic wire, and hence the patterning of refractive index is essential to an integrated photonic technology. We know that the hydrogen content in amorphous silicon can be altered. Hence by using lithography techniques for selected regions, a method for patterning of refractive index in amorphous silicon can be developed [21–23]. Figure 2.2 [24] shows the preparation of a waveguide by photolithographic masking and hydrogen implantation of predeposited hydrogenated amorphous silicon [24].

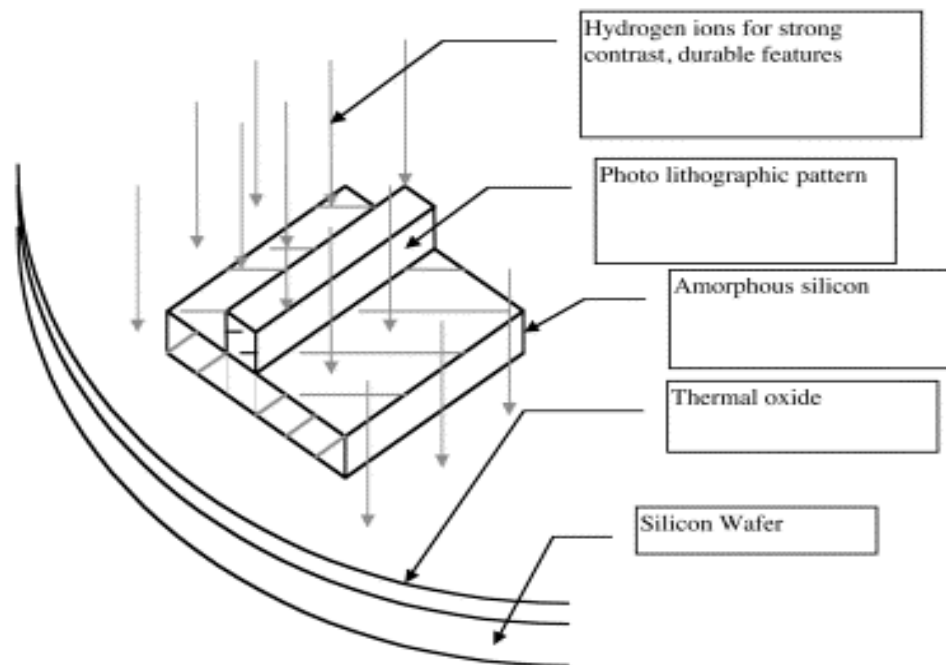


Figure 2.2: Use of photolithography and hydrogen implants to create a refractive index gradient.

The thin films used for my work were prepared by hot-wire chemical vapor deposition method. The films produced by these methods are appealing because the required 1-2 micron thick amorphous silicon films are deposited inexpensively and quickly [25]. These films, having optically smooth surface and due to their low mid-gap defect concentrations have high near-IR transparency [26, 27]. The process of fabricating photonics structure is shown in figure 2.3.

Figure 2.3 further explains some more ideas from our group for fabricating the wave guide structures using masking and hydrogen implant process. As described in [25, 26] hydrogen implantation was carried out at 50, 100, 175 KeV. First amorphous silicon was deposited on a optically smooth glass substrate followed by deposition of 1 micron of metallic film (silver) for stopping hydrogen. Then patterning was done onto the metallic layer using standard photolithographic techniques. Hydrogen was then implanted uniformly throughout the thickness of the layer. The remaining silver is etched out.

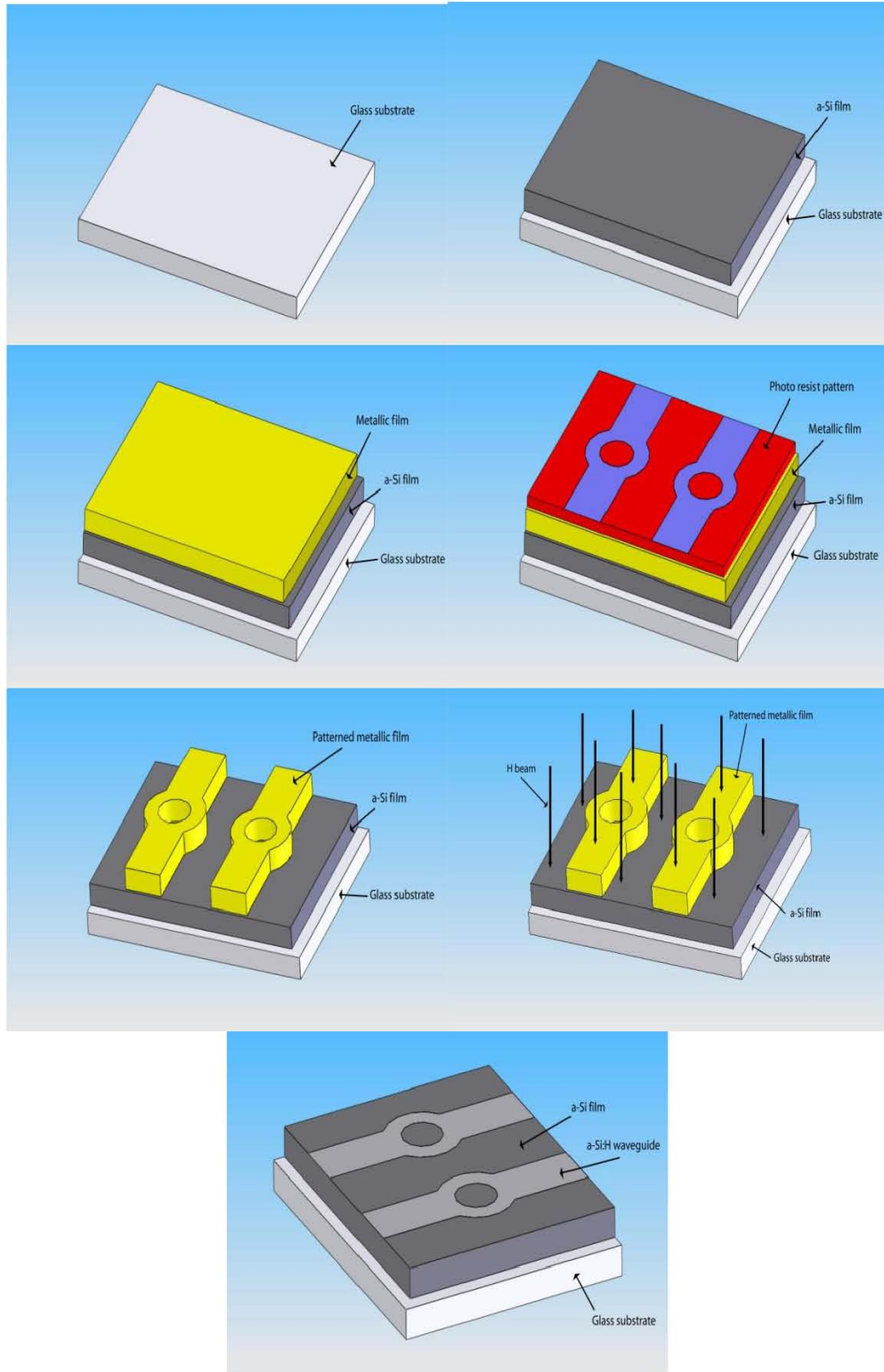


Figure 2.3: Steps to prepare hydrogen implant patterned hydrogenated amorphous silicon films.

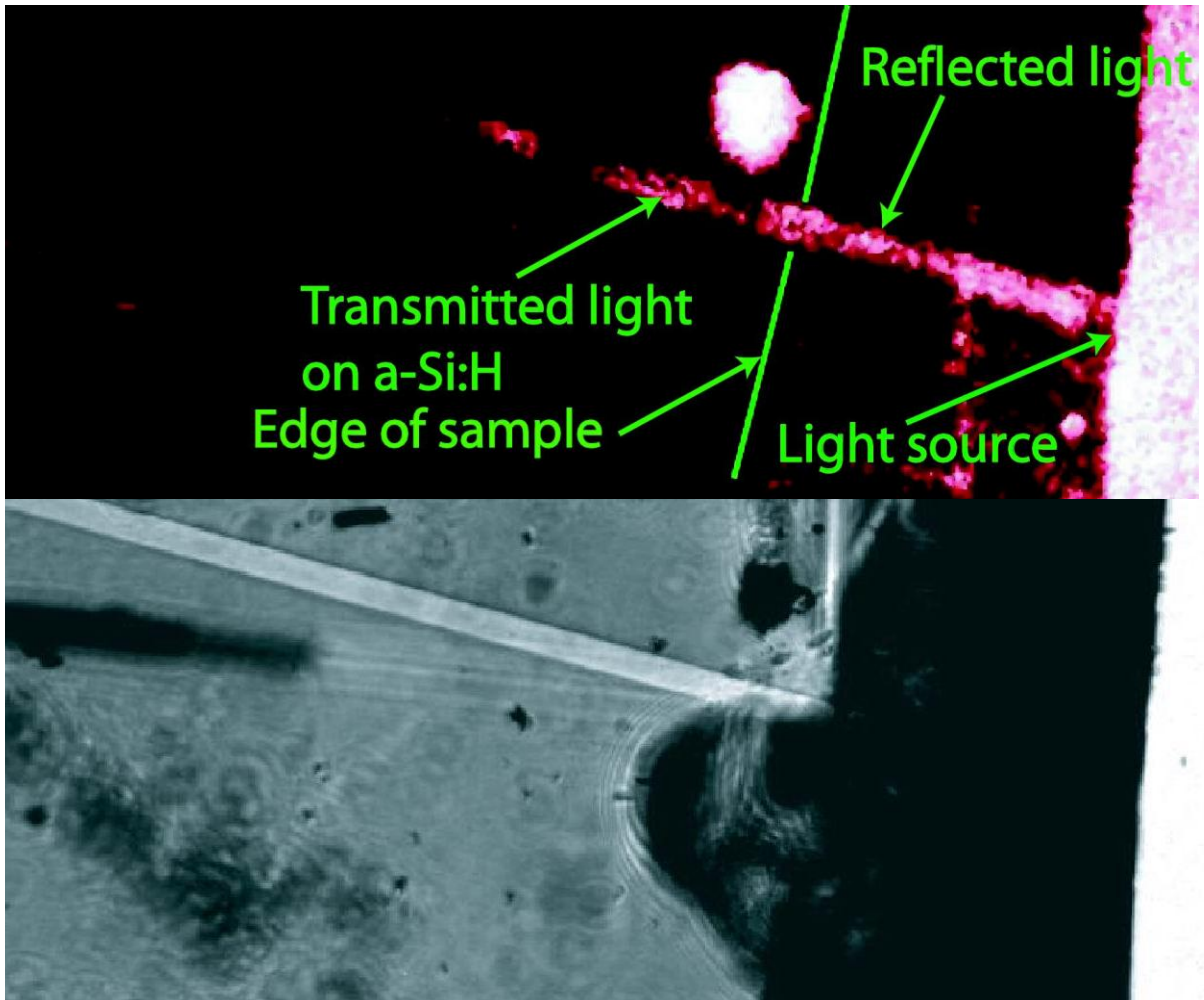


Figure 2.4: Illuminated a-Si:H film

Figure 2.4 shows the operation of a waveguide under laser illumination. A micrograph of the sample with the waveguide (bottom) and the operation of waveguide under visible (633 nm) laser spot illumination (top) are shown.

2.1.5 Light Induced Changes in a-Si:H

Optical illumination and the changes it causes in a-Si:H have been studied for over 25 years because of its wide applications in devices such as thin-film transistors

and solar cells. One of the most widely studied effects is the creation of defects by prolonged illumination by absorbed light. Over more than 25 years a tremendous number of experimental and theoretical investigations have been devoted to this subject, since Staebler and Wronski first showed a slow degradation of solar cells as they were exposed to sunlight.

The light induced changes related to the refractive index of a-Si:H is discussed here. Slow light-induced change in the optical properties of amorphous silicon materials have been studied by Hata *et al.*, [39], who state that high intensity light soaking at temperatures ranging from room temperature to 200⁰C caused a surprising large, reversible change in the optical properties of hydrogenated amorphous silicon films. Hata et al, explained that the dielectric functions of a-Si:H measured as a function of time steadily decreases with increasing light soaking time, indicating that the rate of light-induced change is slow and occurring over a span of many hours. As is the case of any semi-conductors, light absorption in amorphous silicon produces free carriers.

The free carrier mobility and diffusion lengths are small in a-Si:H [38], and become smaller as light exposure time is increased. The diffusion length and mobility are related ($\text{mobility} = D/kT$). Typically the diffusion coefficient and mobility in amorphous silicon are greater for electrons than for holes. Hence, the fast light induced changes may correlate with the observation that carrier transport decreases with light exposure time.

CHAPTER 3

Phononic Hydrogenated Amorphous Silicon

Recent reports demonstrate that phonon properties can be utilized for important technological purposes. For example in 2005 researchers from Intel demonstrated a continuous wave laser on a silicon chip based on the Raman Effect [28]. This achievement furthers the goal of an all optical information conveyance network based on photonic devices. There is an underlying march towards an all-photonic information conveyance and manipulation network. By discovering a laser which can be built inside silicon the researchers believe, the possibility of silicon photonic chips containing dozens or even thousands of hybrid silicon lasers manufactured using low-cost silicon manufacturing techniques may be possible. However those Raman lasers are inefficient. By controlling the flow of phonons these devices may be improved. This PhD work will explore the prospect of controlling material properties, to control the flow of phonons and the applications of phonon flow control to device designs.

3.1 Introduction to Phonons

In many aspects crystalline and amorphous silicon differ, one of the most important aspects is their vibrational properties. Understanding the vibrational properties of a-Si:H, the phonons produced due to these vibrations and the measurement of the

generated phonons by using of Raman spectroscopy is discussed.

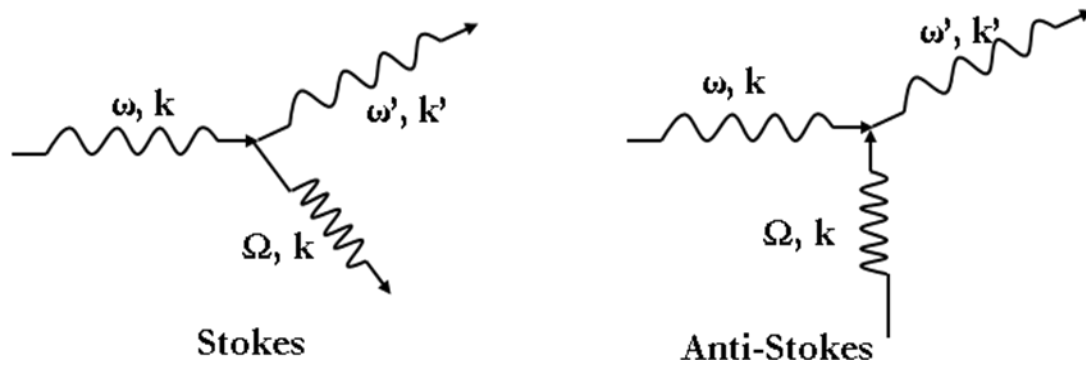


Figure 3.1: Raman scattering of a photon with emission or absorption of a phonon.

Raman scattering involves an incident laser beam of known wavelength onto a sample and measuring the reflected light. In Raman Effect a photon is scattered inelastically by the material with creation or destruction of a phonon. The selection rules for the first order Raman Effect are $\omega = \omega' \pm \Omega$; $k = k' \pm K$. Where ω, k refer to the incident photon; ω', k' refer to the scattered photon and Ω and K refer to the phonon created or destroyed in the scattering event [29]. Figure 3.1 [29] shows the brillouin scattering when an acoustic phonon is involved and polariton scattering when an optical phonon is involved.

The dynamics, generation and decaying of phonons is explored by quite a few researchers. [31] reveals relaxation time constants for 480 cm^{-1} phonons as long as 10ns. Scholten *et al.* have measured the decay of high frequency of phonons [30] at 2K by pulsed anti-stokes Raman experiments, which tells us the decay time for high frequency phonons which are generated by fast carrier relaxation process. Furthermore the transport of phonons in a-Si:H has been explored, the transport is shown

to be governed by elastic scattering with a diffusion coefficient of $1\text{cm}^2/\text{s}$ [32].

Over twenty years of research into the commercially interest amorphous silicon (it is used in flat panel displays and solar cells) have been used for many properties unique to the amorphous phase. Of particular importance to this work is the previously mentioned ability of amorphous silicon to absorb large quantities of hydrogen. This is relevant here because Wakagi et al [33] demonstrated that both the coordination number and the bond length of silicon are a function of the hydrogen control. In turn it is then expected that the propagation and other phonon properties will also be a factor of hydrogen content, since the coordination number and bond length are factors in the local spring constant of the material. For example, the speed of a long wavelength phonon is dependent on the average spring constant [29] and this spring constant is directly linked to coordination number which in turn is H-dependent.

3.2 Phonon Gap and the Hydrogen Dependence

The hydrogen dependence of the band gap has opened the door to continued use of crystalline matrix elements to model the characteristics of amorphous silicon. The amorphous silicon band gap is much larger than the crystalline silicon. The band structure (E-k diagram) of a semiconductor is responsible for the light absorption and emission. In case of direct band gap semiconductors (where the minimum of the conduction band lies at the same wave vector k as the maximum of the valence

band), the light absorption is stronger and is characterized by a larger absorption coefficient. In the case of amorphous silicon, there is an indirect band gap (where the minimum of the conduction band is not lying at the same wave vector k as the maximum of the valence band), having smaller absorption coefficient. In indirect band gap a phonon is required to conserve momentum when an electron is excited from the valence band to the lowest conduction band minimum. Phonons are quantized elastic wave associated with lattice vibrations; it has comparatively low velocity, energy compared to that of a photon. Phonon assisted absorption in indirect band gap materials is shown in figure 3.2 (b) and (c), where case (b) shows the photon absorption assisted by a phonon absorption and case (c) shows the absorption of a photon along with the emission of a phonon. The minimum photon energy that can be absorbed is slightly below the band gap energy in the case of a phonon absorption and is slightly above the band gap in the case of phonon emission [34].

In the discussion above, photonic materials were defined to have a pattern of refractive index varied regions designed to interact with light. Here the possibility of engineering structures to interact with phonon propagation is explored. Generation of phonons due to the incident light in amorphous silicon has been long known. It is important to recognize that phonons in crystals are not localized, however in polycrystalline and amorphous materials where phonons are localized to domains much smaller than the size of the material sample. Semiconductors could be engineered to simultaneously have electronic and photonic bands. Electron wave function dictates electronic band structure, Joannopoulos et al [35] explained that a refractive index heterogeneous material could produce forbidden bands for light

propagation. Fortmann *et al.*, [8] proposed an analogous phononic band when phonon scatterers were distributed in a material.

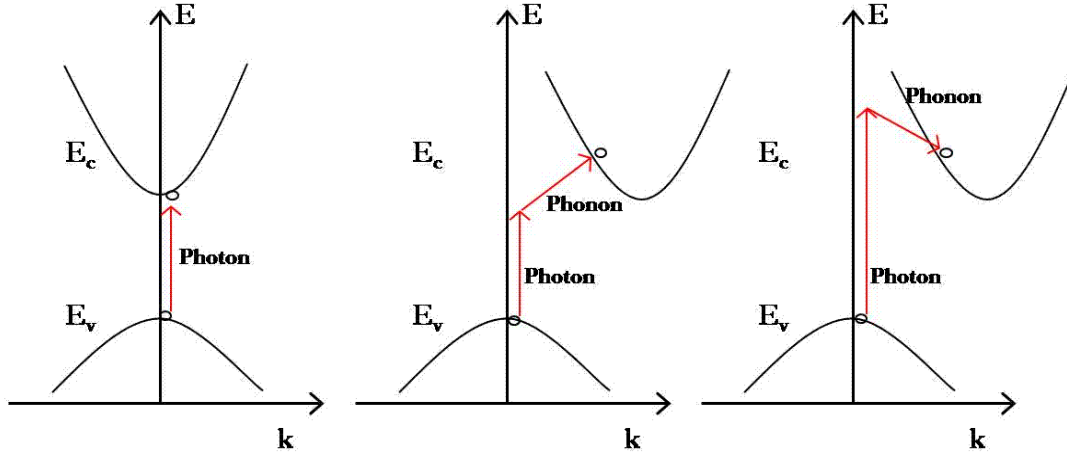


Figure 3.2: E-k diagram. a) Photon absorption for direct band gap semiconductor. b) Photon absorption along with phonon absorption in indirect band gap semiconductor. c) Photon absorption along with phonon emission in indirect band gap semiconductors.

Phononic bands are analogous to photonic bands [8]. Amorphous silicon has a good affinity towards the intake of hydrogen, and by varying the concentration of hydrogen it is possible to make a material with varying refractive index. The a-Si:H band gap has a strong dependence on the Si-H₂ concentration [14]. This allows a-Si:H to have photonic bands and also photon localization. As the energy of phonon is lower than that of a photon, we can say that if a material has a periodic arrangement of regions of differing phonon velocity and atomic vibration spectra exhibit phonon localization, forbidden gaps and bands [8]. Fukitani *et al.*, [14] further mentions that the concentration of Si-H₂ and the related band gap is interesting for three reasons: One is that the silicon atom which is bonded to two hydrogen atoms is

heavier than silicon atom. Two, the spring constant that couples the silicon atom to the lattice has been reduced by almost a factor of two, relative to the average silicon in a-Si:H matrix. Three, the random spacing of the Si-H₂ sites is of the same scale as the phonon wavelength needed for an optical transition. This tells us that the occurring of the phonon band is due to the Si-H₂ sites [8].

Figure 3.3 shows the changes in the crystalline silicon band diagram in order to explain the hydrogen dependence of amorphous silicon band gap [38]. The figure in particular is modified by the short coherent length of electrons and a forbidden band in phonon spectrum arising from interaction of the phonon spectrum with Si-H₂ scattering structures.

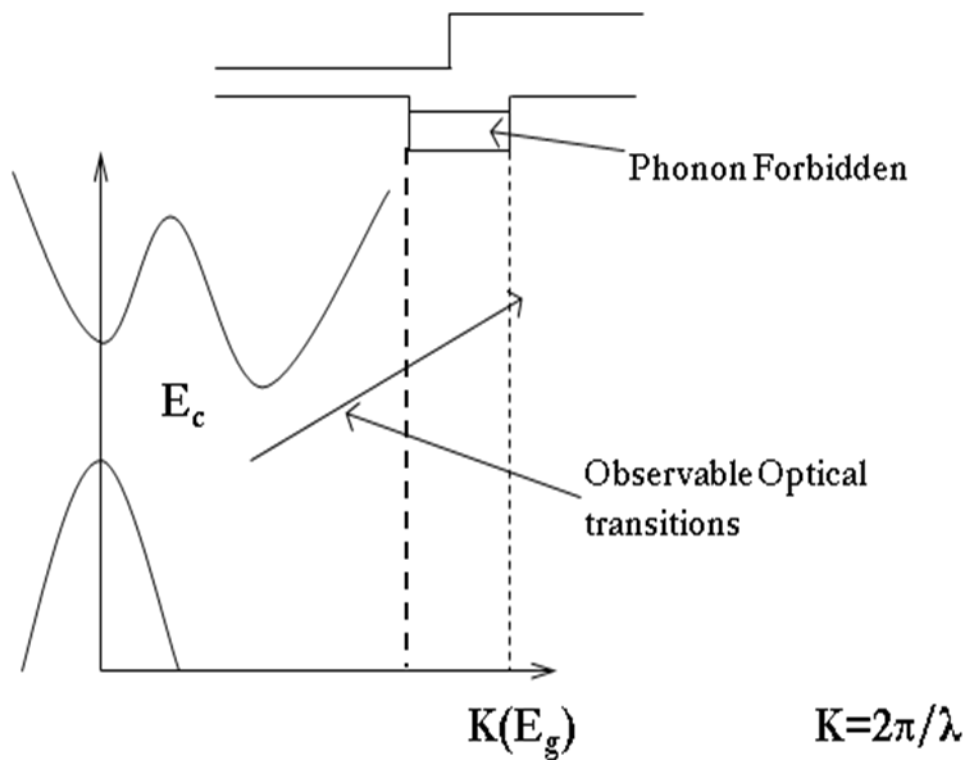


Figure 3.3: Changes in the crystalline silicon band diagram to explain the hydrogen dependence.

3.3 Controlling and Utilizing Phonon Energy

As discussed in earlier sections, the generation of phonons, the phonon life-time, the relation of these to optical band gap and the hydrogen dependence will be explored. Measurements indicate that the phonon life-time is long in amorphous silicon, so its diffusivity may be long compared to the crystalline silicon case.

In this section the first experiments to probe the diffusion length in amorphous materials are described. These experiments were based on Stokes and the anti-Stokes Raman shift. Phonons generated in one location were utilized to produce a Raman shift in another region as described below. We know that the phonon lifetime is considerable long in amorphous silicon so as its diffusivity when compared to the crystalline silicon.

Raman spectrometer was used to probe the phonon diffusion length ($\sqrt{D\tau}$), where D is the diffusivity and τ is the life-time. A Thermo Nicolet Almega Raman spectrometer with 785nm probe beam was used to analyze the amorphous silicon thin films. This research effort employed amorphous silicon films grown at National Renewable Energy laboratories. The amorphous silicon samples were prepared by hot wire CVD [25] with different film thickness. Figure 3.4 shows the schematics of the method used for Raman measurement.

As shown the sample holder has a liquid nitrogen inlet and outlet. To reduce the thermal noises all the measurements were taken at liquid nitrogen temperatures.

A 0.20 mW diode light source connected to a fiber optic lead was used to feed the 470nm bias light to the bottom (glass side) of the amorphous silicon thin film. The use of bias light was to generate phonons which were detected using the spectrometer.

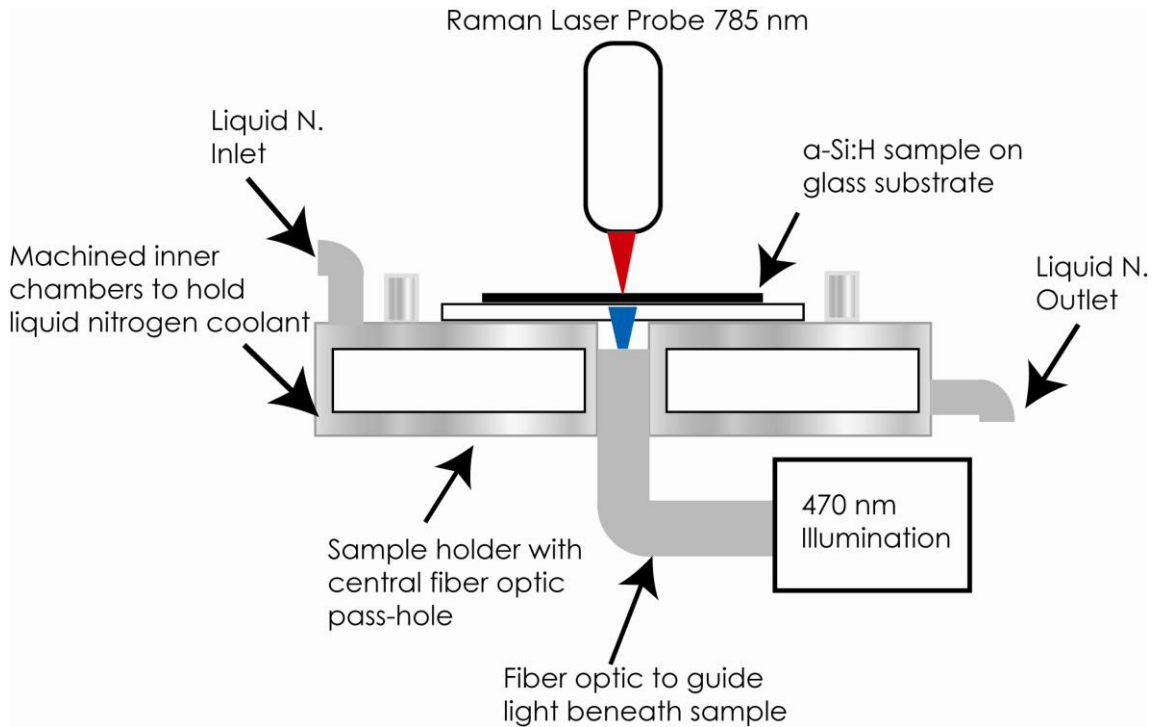


Figure 3.4: Liquid nitrogen cooled sample holder.

Figure 3.5 shows us the comparison of 490cm^{-1} Raman peak as a function of light bias for samples with 2-3% of hydrogen. a-Si:H is an ideal material for phononic engineered devices, because the refractive index can be changed according to requirements; fabrication of these thin films is easily done; known photolithography and etching techniques can be used to prepare waveguides on these films. Phonons generated in these materials have greater lifetimes and their transport is feasible in these films.

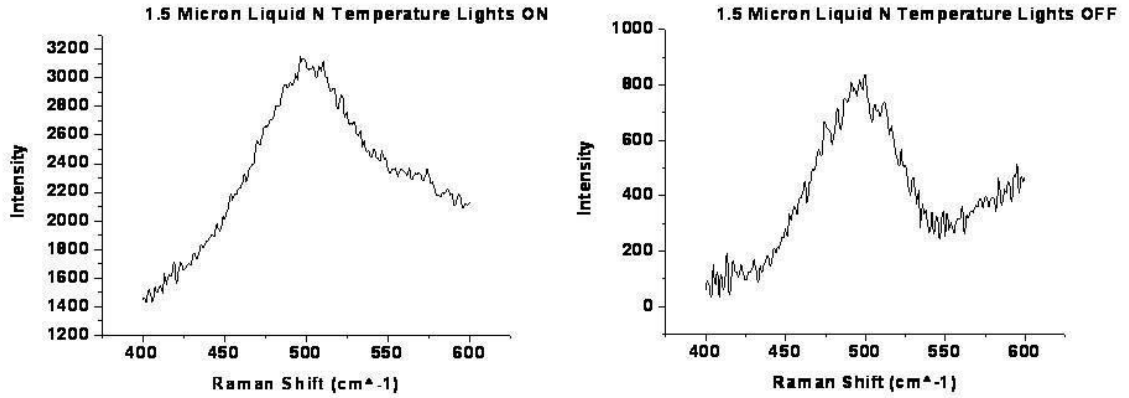


Figure 3.5: Raman spectra for sample with 2-3% hydrogen.

| Thickness | No Bias Light | Bias Light | Change |
|------------------|--------------------------|-----------------------|---------------|
| 1.5 μ | 27229.9 | 51301.6 | 24072 |

Table 3.1: Calculated area under the 490cm⁻¹Raman Peak.

Data analysis focused on the 490 cm⁻¹ Raman peak as a function of light bias. Figure 3.5 shows the Raman spectra of samples as a function of light bias. The increased bias light induced response for these samples is consistent with phonon diffusion lengths greater than 1.5 μ m and probably much greater. It is also important to note that the increased bias light response is not consistent with bias light leakage or bias light induced photoluminescence contributions to the Raman spectrum. However a photoluminescence contribution was not directly investigated.

Figure 3.6 shows device concept designed to modify a light beam traveling in waveguide-1 by Raman shift (anti-Stokes) whenever a light beam in waveguide-2 is present. Waveguide-2 phonons, generated by Stokes-shift and recombination of photo-carriers, cross the phonon bridge to shift a portion of the light in waveguide-1. Fabrication techniques for a phonon wave-guide (and concentrator) employ hydrogen implantation to reduce the phonon speed in the core of the guide relative to its cladding. Hydrogen implantation (in this case for refractive index patterning) has been previously described [24].

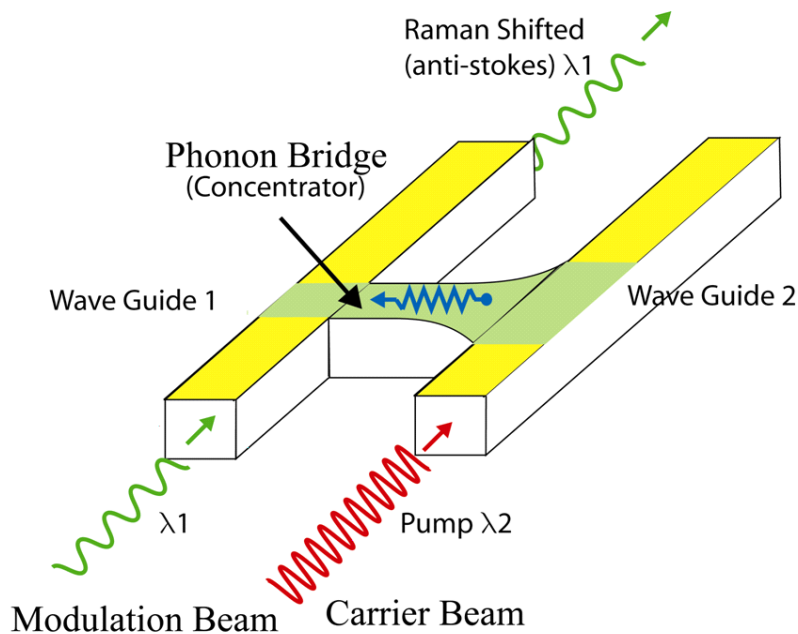


Figure 3.6. Using an amorphous silicon bridge phonons induce an anti-Stokes shift in the first beam whenever a second beam is present in waveguide 2. The magnitude of the shift is proportional to the magnitude of each of the beams and the shift itself is a function of the amorphous material used for the bridge.

The phononic properties of amorphous silicon have been examined. The localization of phonons in domains offers an explanation for the reported long phonon lifetime, large diffusion coefficient, and relatively long phonon diffusion length in amorphous silicon. A Raman-based device was developed that modifies a first light beam by a second light beam without electronic components. Such devices could be prepared using previously described processes designed for the refractive index patterning of amorphous silicon. Importantly, the understanding of phonon transport is of broad application including neural transport.

Chapter 4

a-Si based Solar Cells: Spectral Modifications

4.1 Solar Spectrum

The basic principle for the functioning of a Solar cell is the photo-induced electron transition from a valence band to the conduction band (band gap) of a semiconductor, in solar cells a part of energy from the sun excites the electrons in the valence band. These electrons are excited by photon energies equal or higher than the band gap of the material. Photons with less energy than the band gap pass through without interacting with the electron and without power generation. Every semiconductor with suitable conditions is capable of this transition. The main property required for this transition to occur is the presence of some kind of internal electric field that is able to separate the freed electrons and holes so that they can pass out of the material into the external circuit before they recombine (such as doping in different regions, contacts, different surfaces). The flow of carriers into the external circuit constitutes a reverse electrical current density (J amp cm^2), which under short-circuit conditions, is known as the short-circuit current density (J_{sc}) [41]. During this, there is separation of charges; this separation sets up a forward potential difference (ϕ) between the two ends of the material, under open

circuit conditions this potential is known as the open circuit voltage (φ_{oc}). To maximize a solar cell's performance, it is desirable to increase both J_{sc} and φ_{oc} . For a semiconductor to have large value of J_{sc} , the material should have a small band-gap with high absorption over a wide energy range and to have material properties such that the photo excited electrons and holes are able to be collected by the internal electric field and pass into the external circuit before they recombine [41]. For φ_{oc} to be maximum, it is preferred to have forward current driven by the photo-induced potential difference be as small as possible, since this current will reduce the potential difference set up by the light.

Figure 1.1 from reference [41] tells us about the average solar spectrum at the surface of the earth, with band gap of various semiconductors indicated. In this chapter I will be explaining the semiconductor band gap and the related photon energies, further focusing on amorphous silicon (a-Si) based solar cells. The past, present and future works on a-Si solar cells and the idea/results of exploring silicon nano particle for spectral modifying layers for higher efficiency of the solar cells have been discussed.

For an electron to jump from valence band to the conduction band requires energy. In any conventional solar cell the main idea is to absorb as many photons from the solar radiation as possible. This further leads to analyze the solar spectrum. Figure 4.2 tells us the intensity of solar radiation varying with the wavelength. Most of the solar energy occurs in the region of 0.3 – 0.7 micrometer range and the rest spread in a wide range of spectrum.

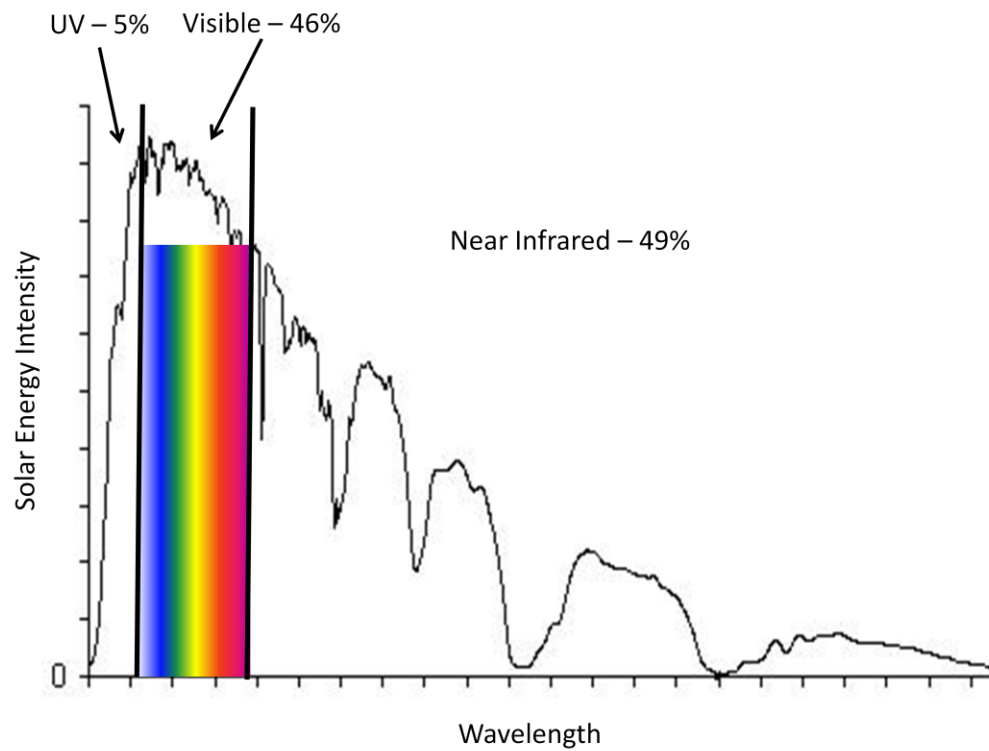


Figure 4.2: Solar intensity varying with the wavelength.

The key for a good Solar cell is to utilize as much as radiation as possible. The ratio of the number of charge carriers collected by the solar cell to the number of photons of a given energy incident on a solar cell is its quantum efficiency. In an ideal case, if all the photons of a certain wavelength are absorbed and the resulting minority carriers are collected, then the quantum efficiency at that particular wavelength is unity. Figure 4.3 shows the quantum efficiency curve of a silicon solar cell.

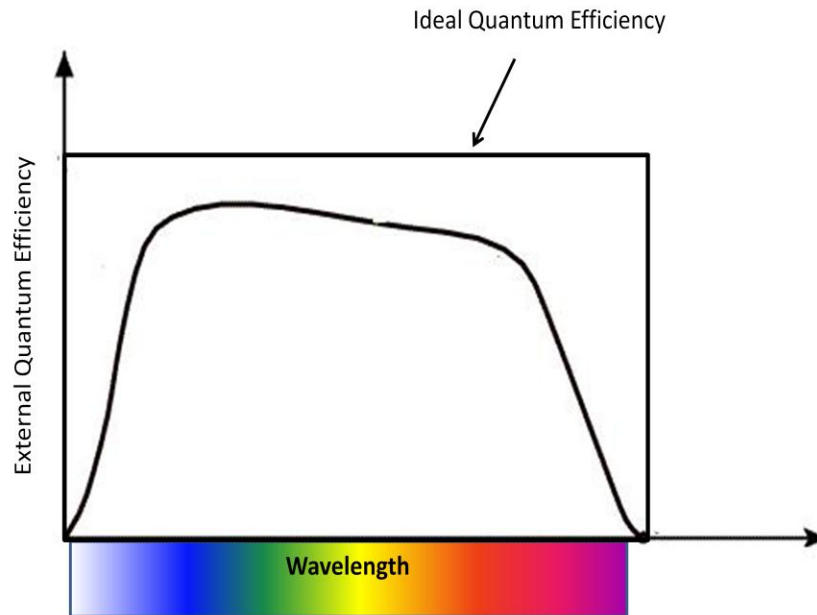


Figure 4.3: The quantum efficiency of a silicon solar cell.

Ideally the quantum efficiency value is fairly constant across the entire spectrum, however for most solar cells it is reduced of the effect of recombination, where the charge carriers were not able to move into an external circuit [43, 44]. For example, the front surface passivation affects the charge carriers generated near the surface, and since blue light is absorbed very close to the surface, high front surface recombination will affect the "blue" portion of the quantum efficiency. Similarly, green light is absorbed in the bulk of a solar cell and a low diffusion length will affect the collection probability from the solar cell bulk and reduce the quantum efficiency in the green portion of the spectrum [44]. Quantum efficiencies are of two types, external quantum efficiency, where in the effects of optical losses such as reflection and transmission are included internal quantum efficiency, which refers to the efficiency with which light not transmitted through or reflected away from the cell can generate charge carriers [43, 44].

The entire energy spectrum of sunlight from infrared to ultraviolet cover a range of about 0.5 to 2.3 eV[43]. Figure 4.4 [45] gives us an idea of few photovoltaic materials with different energy band gaps, we see that the photons with equal band gap energy gets absorbed by the material where as photons with less energy than the band gap pass through the material.

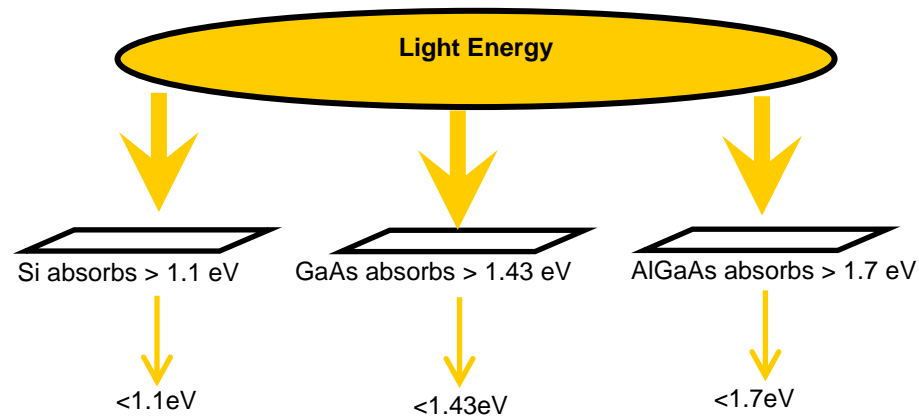


Figure 4.4: Light absorption and transmission of different photovoltaic materials.

As the need for higher efficiency solar cell is getting stronger, various research groups across the globe are working on utilizing the whole spectrum. Presently the solar cells which are designed use less of the UV photons (5%) from the sun's radiation.

4.2 a:Si based solar cells

Silicon has dominated the electronic industry since half a century. Owing to its abundance in the earth's crust, the stability, non-toxicity and the wide level of research done, it is an ideal material for Photovoltaics. Silicon has an almost ideal band gap for a solar cell energy conversion figure 4.4. The cost of crystalline Silicon solar cells is greater than that of its closest competitors [41], also they require very high material quality where as amorphous silicon are gaining momentum in the solar market. Amorphous silicon is a thin-film material without long range atomic order which can be deposited by a variety of techniques suitable for large scale production [41]. Amorphous silicon based solar cells uses ultrathin layers of a-Si (0.2 microns), and can be easily deposited on inexpensive substrates such as glass, flexible plastic or stainless steel. This means they use very less amount of raw material (silicon) compared to the crystalline Silicon. Table 4.1 further tells us the comparisons of amorphous silicon based solar cells against the crystalline silicon solar cells.

| | aSi/SiGe | C-Si |
|----------------------------------|--|--|
| Grain Size (μm) | Amorphous | Single Crystal |
| Typical Growth Methods | CVD | epitaxy + “epi-lift” “smart-cut” |
| Rates ($\mu\text{m}/\text{m}$) | 0.01-0.1 | 1-10 |
| Efficiencies (%) | 8-13 | ~18 |
| Cell Thickness (μm) | 0.3-0.7 | 5-50 |
| Pros | very high absorption, E_g tailoring | infrastructure, Synergy with IC industry |
| Cons | instable (SWE), Poor red collection | 3 step process, Large area difficult |

Table 4.1: Current amorphous and thin-film approaches.

4.2.1 a:Si based solar cells and multi-junction approach

The adaptability of amorphous silicon based solar cells to the technique of stacking layers, in which different layers are responsive to a different color in the spectrum, makes it one of the widely used materials for the multi-junction solar cell approach. aSi based solar cells have two main ingredients silicon and hydrogen, which are easily available and environment friendly. Alloys of hydrogenated amorphous silicon (a-Si:H), particularly with C or Ge, play an important role [46] to approach higher efficiency in power generation. a-Si alloys degrade upon light soaking [47] due to the Staebler-Wronski effect (SWE), and the band tails and other structural defects in the form of weak, dangling bonds affect the transport of photo-carriers in the solar cell. To overcome these problems, researchers are working on the multi-junction approach. These multi-junction materials used are of different band gaps that also increase the overall spectral response of the device and results in higher efficiency. These junctions typically employ

roughened front surfaces to produce a myriad surface relative to the incident light and to scatter this light to large angles.

One such example of multi-junction approach is the alloy of a-Si:H and Ge. Smith et al., [48] investigated the performance of a-Si:G:H solar cells as a function of the band-gap between 1.2 and 1.7 eV, finding that the solar cell performance drops sharply if the band-gap is smaller than 1.5 eV. Such a decrease in performance with the increasing Si/Ge ratio may be due to the decrease in band-gap, or it may be intensified by an increase in defect density or a widening of the valence band tail with increasing Ge [41, 49]. United Solar Systems Corp., is one of the leading companies which is working on these types of solar cells. Yang et al., have achieved an initial active area (0.025cm^2) efficiency of 14.6% for a a-Si:H/a-SiGe:H/a-SiGe:H triple junction solar cells. Figure I of reference [50] gives us a schematic of a triple junction solar cell [50].

The top cell in figure 1 of reference [50], is a Si:H material (band-gap of 1.8 eV) absorbs blue photons, the middle and bottom cells use a-Si:Ge:H alloys (band-gap ~ 1.6 and 1.4) of different Si to Ge ratios absorb green and red photons [50]. Yang et al., reported that they have achieved cell efficiencies of 14.6% [50, 51]. The spectrum-splitting multi junction solar cells are maturing very rapidly with many ideas being worked on to trap the solar radiation. One such unique approach is discussed in the following sections.

4.3 Silicon nanoparticles and Solar cells

Calham et. al, reported in early 1990 about the observation of photoluminescence (PL) from porous silicon consisting of silicon nanoparticles and nanowires [52]. The idea of

room temperature PL of silicon nanoparticles has opened up research and development in the areas of optoelectronic devices such as light emitting devices, thin film electroluminescence displays, solar photovoltaic devices, single-electron devices, non-volatile memory and lasers [53-59]. The idea in this work is to find a way using amorphous silicon solar cell in junction with a thin layer of silicon nanoparticles to enhance the output power of solar cells. In this section I will be discussing the properties and sizes of silicon nanoparticles which are currently being used for the solar cell research.

4.3.1 Photo-luminescence of Silicon nanoparticles

Silicon nanoparticles emit visible light (luminescence) when irradiated with ultraviolet light. This emission is dependent on the size of the nanoparticles. Such property of silicon nano powder makes it significantly different from bulk crystalline silicon. I will be further discussing the uses of these particles in solar photovoltaic devices. Silicon nanoparticles are produced by a variety of different methods such as aerosol techniques [60, 61], plasma deposition [62], sputtering [63, 64] and ion implantation [65] followed by high temperature annealing.

Several groups have developed silicon nanoparticles in large quantities at low cost, which provides a huge possibility for commercial applications. CO₂-laser-induced decomposition of Silane (SH₄) in a gas flow reactor has been shown to be very useful for the synthesis of large quantities of silicon nanoparticles [53, 66 and 67]. Research group of Prof. Mark Swihart (State University of New York at Buffalo) has been working on one of such methods preparing Silicon nanoparticles smaller than 5nm [68, 69]. In my

discussion with Prof. Swihart, he guided me regarding the typical etching process of Silicon nanoparticles. The products of gas-phase decomposition are etched with a mixture of Nitric acid (HNO_3) and Hydro fluoric acid (HF). The particles having oxide layer at the beginning will be oxidized by HNO_3 and then etched by HF. This etching process takes usually minutes and the etching rate is controlled by varying amount of methanol used to initially disperse the particles [70]. The etching time is significant as it is related to PL [68].

Belomoin et al., have demonstrated the PL of Silicon nanoparticles using Ultraviolet (UV) source of 365nm. They demonstrated blue to red emission from their silicon solution in figure 3 of reference [71].

4.3.2 Reasons for Photoluminescence in Silicon Nanoparticles

Extensive research has been going on in the field nano-sized structures of semiconductor materials since visible PL was observed in nanometer-sized silicon. Research groups are working on theoretical as well as experimental approaches to study and clarify the mechanism of PL particularly in silicon nanocrystals. However, there are still intensive debates on several major issues, including the origin of the PL, the variation of the optical gap as a function of the nanoparticles size, and the effect of oxygen contaminants on optical properties of silicon nanoparticles, which are not independent with each other [53]. These debates are mainly on the issues of the nature of excitations and the origin of stokes shifts between the PL emission and the absorption band-gap found in small silicon nanoparticles.

To understand the origin of visible PL and other electronic properties, it is necessary to study the silicon nanoparticles of various sizes and also to understand the role of surface recombination. Yoffe et al, [72] showed that the optical absorption energy gaps as in agreement with calculated values, which are determined by quantum confinement effects for silicon nanoparticles. Some researchers agree that the PL occurs following the excitation coming from the free exciton recombination, i.e., it is quantum confinement that determines the PL energy [52]. These studies leads us to the better understand of quantum confinement of electrons and holes in indirect band-gap semiconductors, which at present is much less understood [73, 74]. Researchers have demonstrated that the exciton nature of luminescent states is responsible for the light emission from porous silicon [75], also in a model proposed by wolkin et al., [76] describes that the excitation by high energy photons results in the creation of electron-hole pairs in the nanocrystalline phase in porous silicon. Silicon, being an indirect band-gap material, researchers are debating whether this excition recombination is direct or indirect transition. Wilcoxon et al., [77] reported that the optical absorption showed both indirect and direct band-gap transition feature, and these transitions exhibited different quantum confinement effects. The indirect band-gap shifts from 1.1eV in the bulk to ~2.1eV for nanocrystals (~2nm), and the direct transition at Γ blue shifts by 0.4eV from its 3.4eV bulk value over the same range as shown in figure 6 of reference [77].

Many other research groups however, have found the excition recombination to be indirect in nature. Kovalev et al., [78] observed PL with a set of narrow peaks associated with silicon transverse acoustic (TA) and transverse optical (TO) momentum conserving phonon-assisted optical transitions, which show that light emission from

silicon nanocrystals behave as indirect band-gap semiconductors. There are more evidences that the silicon nanocrystals retain the indirect character for the transitions relating to the minimum gap and as schuppler et al., [79] points out, the PL intensity from indirect band-gap materials can be low.

4.3.3 Raman Spectra of Silicon Nanoparticles

As discussed in previous section a strong PL has been observed in the silicon nanoparticles and extensive experimental and theoretical studies have been done on optical and structural properties of these materials. Although there are ongoing debates about the origin of PL, the prospect of realizing light-emitting devices stimulated intensive research of various nanometer-sized, Si based structures using different types of preparative methods [80].

Particles of nanometer size show low wave-number vibrational modes, these modes can be observed by Raman Spectroscopy (RS) which makes it a powerful technique. Silicon in general is known to have an exceptionally large Raman shift. Silicon based Raman laser has been demonstrated by Rong et al., [81]. Rupp et al., [82] have studied the Spark-processed silicon which shows strong photoluminescence in the blue and the green region of the visible spectrum, the relationship between the presence and size of Si nano particles and PL emission wavelengths has been analyzed using Raman scattering.

Fortmann et al., [83] showed that as the domain size decreases the silicon band-to-band absorption is reduced (for a given wavelength). Silicon nano particles may have

an even larger potential to induce Raman shift since (when the particles are sufficiently large to support a given phonon mode) each particle contain a given mode and phonon lifetimes are long compared to crystal. Since long wavelength phonon decay products are not possible in nanometer sized particles and since in amorphous (and particle) silicon the phonon lifetime is exceptionally large (84, 85) when compared to single crystal silicon or other materials. Therefore the photon produced by one photon-phonon energy exchange is likely to be available for a second photon energy increasing phonon-photon energy change (Raman scattering a.k.a. anti-Stokes shift). Silicon nano particle-based Raman up and down conversion offers the best prospect for solar cell back surface applications (since, the strongly absorbed visible light is removed prior to encountering the silicon nano-particles parasitic light absorption by the particles is reduced). Therefore, it is reasonable to expect that silicon nano-particles will not absorb visible light as strongly as bulk silicon. Furthermore, silicon nano-particles are known to strongly luminescence in the visible under UV illumination [86]. This luminescence may be related to uncertainty ($\Delta k \Delta x \geq 1/2$) relaxation of crystal silicon k conservation laws due to the small particle size ($\Delta x \sim 5nm$) and the fact that an oxide coated silicon nano-particle may have few or no defect recombination sites through which photo excited carriers can recombine non-radiatively [82].

Interestingly, silicon nano-particles also offer the prospect of IR up-conversion through Raman (anti-Stokes) scattering. Silicon in general is known to have an exceptionally large Raman shift. Silicon nano particles may have an even larger potential to induce Raman shift since (when large enough to support a given phonon mode) each particle would contain a given mode and phonon lifetimes may be long compared to

crystal. Since long wavelength phonon decay products are not possible in nanometer sized particles. Silicon nano-particle-based Raman up and down conversion offers the best prospect for solar cell back surface applications (since, the strongly absorbed visible light is removed prior to encountering the silicon nano-particles).

Chapter 5

The idea to use silicon nano particle thin-film layer in junction with commercially available thin-film solar cells is explored. As discussed in chapter 4, section 4.3.1 Silicon nanoparticles emit visible light due to photo-luminescence when irradiated with ultraviolet light. Silicon nano-particles offer relatively low absorption and the potential to convert UV to visible via luminescence and IR to visible via multiple Raman shifts. Experiments we carried out to understand in detail the light scattering and spectral conversion of silicon nanoparticles.

As discussed in chapter 4, section 4.2, the solar spectrum is mainly divided into the visible, ultra violet (UV) and infrared (IR) components. The peak solar emission is in the visible range. Most of the commercially available solar cells use the visible part (~46%) of the spectrum for conversion of photons into electrical current. Rest of the spectrum, the UV and the IR, are transparent to the solar cells. For example single junction amorphous silicon solar cell with semiconductor band gap of ~ 1.7 eV converts photons with wavelengths ranging from ~560nm to 650 nm with near 100% efficiency [87]. Thin-film amorphous silicon solar cells (~200nm thick) have small quantum efficiency at long wavelengths (>700nm) due to low absorption coefficient combined short path lengths in the absorbed layers [88].

Phosphors for modifying spectra's have been around for a long time. Phosphors are considered in the application of up-converting phosphors on the back of solar cells to

up-convert and scavenge the near IR that could not be absorbed in its first path through the solar cell [89]. In this work the considerations necessary for applying a up-converting phosphor to the front of the solar cell will be explored [88].

5.1 Theoretical considerations

An illustration of a light scattering and spectral modifying layer applied to a solar cell is shown in figure 5.1. Figure 5.1 shows the arrangement of Si-nanoparticles diffuse rear reflection used with an amorphous silicon solar cell. The near matching refractive index of amorphous silicon to TiO_2 enables scattered light in TiO_2 to maintain large angles when transmitted into the amorphous silicon.

Here the prospect of silicon nanoparticle based spectral modification is studied. For a given wavelength, as the domain size decreases the silicon band-to-band absorption is reduced [83]. So, we can say that silicon nanoparticles will not absorb visible light as strongly as bulk silicon. Interestingly, silicon nano-particles also offer the prospect of IR up-conversion through Raman (anti-Stokes) scattering. Silicon in general is known to have an exceptionally large Raman shift. Silicon nano particles may have an even larger potential to induce Raman shift since (when large enough to support a given phonon mode) each particle would contain a given mode and phonon lifetimes may be long compared to crystal. Since long wavelength phonon decay products are not possible in nanometer sized particles. Silicon nano particle-based Raman up and down conversion offers the best prospect for solar cell back surface applications (since, the strongly absorbed visible light is removed prior to encountering the silicon nano-particles).

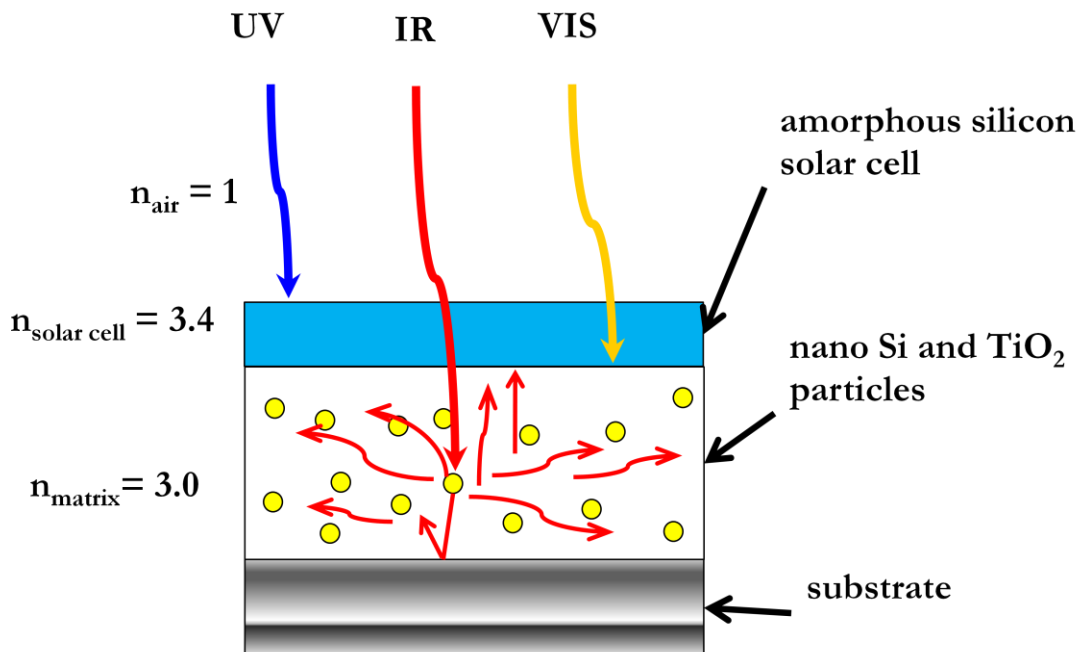


Figure 5.1: Key elements of a Raman-based photon energy up-converting nano-particle silicon dispersed in TiO₂ matrix applied to the back of a solar cell.

5.2 Light diffusivity in a thin-film semiconductor.

It is evident that Silicon nano-particles produce larger magnitude Raman shifts when compared to bulk crystal silicon and that the anti-stokes-to-stokes shift ratio in nano-particle silicon is much greater than that of bulk crystal. This is understandable in terms of the energy needed for the photon up-conversion process. Nano-silicon particles may beat (relative to the ambient) due to extraneous photon absorption. Also, phonons generated by a prior photon down conversion event may exist long enough to contribute to a subsequent photon up-conversion event. Long Phonon lifetime in small domain silicon (nanoparticles in this case) may be inferred from the long phonon lifetimes observed in amorphous silicon.

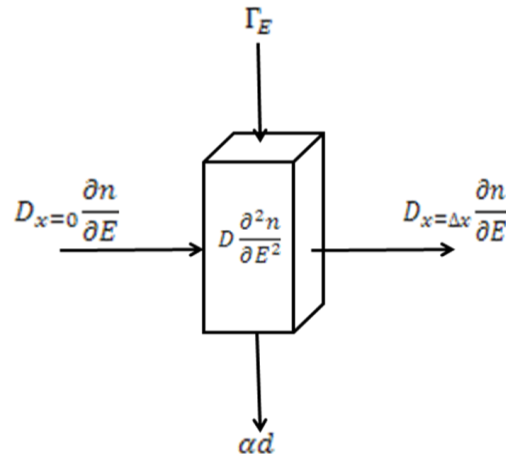


Figure 5.2: Light diffusion into a thin-film semiconductor.

Raman scattering moves photon energies to both up and down in energy. Nonetheless, by analogy to Brownian-motion of airborne dust particles, such random walks (in energy in the cases here) produce some photons of increased energy. After many transits through the silicon particles the long wavelength light spectrum will be broadened by the multiple Raman scattering events. On average a photon attains an (energy) distance from its initial position (in one dimension) equal to $\sqrt{N} \times \Lambda$, where N is the number of hops and Λ is the hop distance. Here, the appropriate consideration is a sum Raman up and down conversions leading to an average energy distance from the initial spectrum.

Light undergoing two Raman shifts has, on average, an energy spread that moves approximately 1.41 times the energy per Raman shift, approximately 0.06eV for the case of Silicon particles. Half of the distribution increasing in energy. A solar cell with good conversion efficiency (e.g., on 0.25 nm thick amorphous silicon solar cell with effective light scattering) for wavelengths up to approximately 800nm would realize an

approximate 5% increase in its power generation due to Raman shifts spectral modifications.

The one-dimensional diffusion constant, D , a random walking particle system is

$$D = \frac{1}{2} \Gamma l^2 \text{ --- (5.1)}$$

Where Γ is the standard hop rate and l is the hop distance. Applying this to Raman up and down energy shifts is direct; with Γ equating with the Raman induced energy hop rate (Raman scattering probability per unit photon path length, β , times photon path length d) and equating l with the Raman scattering induced energy shift (~ 0.06 eV for silicon particles). A simplified diffusion formula such as

$$D \frac{\partial^2 n}{\partial E^2} + \frac{n}{\tau} + \Gamma_E = 0 \text{ --- (5.2)}$$

Considering the diffusivity equation for light falling onto a thin-film, we have

$$\frac{\partial^2 \eta}{\partial E^2} - \frac{\eta}{D\tau} + \frac{\Gamma_E}{D} = 0 \text{ --- (5.3)}$$

Where,

$$\frac{\Gamma_E}{D} = \text{Input}, \quad \frac{\eta}{D\tau} = \text{Recombination}, \quad \frac{\partial^2 \eta}{\partial E^2} = \text{Going Out}$$

D = Diffusion Constant ($\text{cm}^{-2}\text{sec}^{-1}$)
 η = Electron Density (cm^{-3})
 τ = Lifetime of a Photon (sec)
 Γ = Photon Flux ($\text{photon cm}^{-2}\text{sec}^{-1}$)

Here, considering two conditions, the electron density (η) is zero at $E=E_G$ given by eq. 5.3 and the diffusion constant times the rate at which an electron diffuses at E_{\min} , is zero given by eq. 5.4.

$$1) \eta_{E=E_G} = 0 \text{ --- (5.4)}$$

$$2) D \left(\frac{\partial \eta_E}{\partial E} \right)_{E_{min}} = 0 \text{ --- (5.5)}$$

The current density J (Acm⁻²) is,

$$J_{E=E_G} = D \frac{\partial \eta_E}{\partial E} \text{ --- (5.6)}$$

The general solution for eq. 1 is

$$\eta_E = A e^{\frac{-E}{\sqrt{D\tau}}} + B e^{\frac{E}{\sqrt{D\tau}}} + C \text{ --- (5.7)}$$

For eq. 5 the particular solution is

$$\eta_p = C$$

$$\begin{aligned} \Rightarrow \frac{\partial \eta_p}{\partial E} &= 0 \\ \Rightarrow \frac{\partial^2 \eta_p}{\partial E^2} &= 0 \text{ --- (5.8)} \end{aligned}$$

From eq. 5.3 and eq. 5.8

$$0 - \frac{C}{D\tau} + \frac{\Gamma_E}{D} = 0$$

$$\Rightarrow C = \Gamma\tau \text{ --- (5.9)}$$

$$\Rightarrow \eta_E = A e^{\frac{-E}{\sqrt{D\tau}}} + B e^{\frac{E}{\sqrt{D\tau}}} + \Gamma\tau \text{ --- (5.10)}$$

From eq. 5.4 and eq. 5.10

$$\eta_{E=E_G} = A e^{\frac{-E}{\sqrt{D\tau}}} + B e^{\frac{E}{\sqrt{D\tau}}} + \Gamma\tau = 0 \text{ --- (5.11)}$$

From eq. 5.5 and eq. 5.10

$$D \left(\frac{\partial \eta_E}{\partial E} \right)_{E_{min}} = \frac{-A}{\sqrt{D\tau}} e^{\frac{-E_{min}}{\sqrt{D\tau}}} + \frac{B}{\sqrt{D\tau}} e^{\frac{E_{min}}{\sqrt{D\tau}}} = 0$$

$$\Rightarrow A = B e^{\frac{2E_{min}}{\sqrt{D\tau}}} \text{ --- (5.12)}$$

From eq. 5.11 and eq. 5.12

$$\eta_{E_G} = B e^{\frac{2E_{min}}{\sqrt{D\tau}}} e^{\frac{-Eg}{\sqrt{D\tau}}} + B e^{\frac{Eg}{\sqrt{D\tau}}} + \Gamma\tau = 0$$

$$\Rightarrow B = \frac{-\Gamma\tau}{e^{\frac{2E_{min}}{\sqrt{D\tau}}} e^{\frac{-Eg}{\sqrt{D\tau}}} + e^{\frac{Eg}{\sqrt{D\tau}}}} \quad \text{--- (5.13)}$$

From eq. 5.12 and eq. 5.13

$$A = \frac{-\Gamma\tau e^{\frac{2E_{min}}{\sqrt{D\tau}}}}{e^{\frac{2E_{min}}{\sqrt{D\tau}}} e^{\frac{-Eg}{\sqrt{D\tau}}} + e^{\frac{Eg}{\sqrt{D\tau}}}} \quad \text{--- (5.14)}$$

From eq. 5.10, eq. 5.13 and eq. 5.14

$$\eta_E = \frac{-\Gamma\tau e^{\frac{2E_{min}}{\sqrt{D\tau}}} e^{\frac{-E}{\sqrt{D\tau}}}}{e^{\frac{2E_{min}}{\sqrt{D\tau}}} e^{\frac{-Eg}{\sqrt{D\tau}}} + e^{\frac{Eg}{\sqrt{D\tau}}}} - \frac{\Gamma\tau e^{\frac{E}{\sqrt{D\tau}}}}{e^{\frac{2E_{min}}{\sqrt{D\tau}}} e^{\frac{-Eg}{\sqrt{D\tau}}} + e^{\frac{Eg}{\sqrt{D\tau}}}} + \Gamma\tau \quad \text{--- (5.15)}$$

Simplifying eq. 5.15

$$\eta_E = \frac{-\Gamma\tau e^{\frac{2E_{min}}{\sqrt{D\tau}}} e^{\frac{-E}{\sqrt{D\tau}}}}{e^{\frac{Eg}{\sqrt{D\tau}}} \left(e^{\frac{2E_{min}-1}{Eg}} + 1 \right)} - \frac{\Gamma\tau e^{\frac{E}{\sqrt{D\tau}}}}{e^{\frac{Eg}{\sqrt{D\tau}}} \left(e^{\frac{2E_{min}-1}{Eg}} + 1 \right)} + \Gamma\tau \quad \text{--- (5.16)}$$

Differentiating eq. 5.16

$$\frac{\partial \eta_E}{\partial E} = \frac{\Gamma\tau e^{\frac{2E_{min}}{\sqrt{D\tau}}} e^{\frac{-E}{\sqrt{D\tau}}}}{e^{\frac{Eg}{\sqrt{D\tau}}} \left(e^{\frac{2E_{min}-1}{Eg}} + 1 \right) \sqrt{D\tau}} - \frac{\Gamma\tau e^{\frac{E}{\sqrt{D\tau}}}}{e^{\frac{Eg}{\sqrt{D\tau}}} \left(e^{\frac{2E_{min}-1}{Eg}} + 1 \right) \sqrt{D\tau}} \quad \text{--- (5.17)}$$

Simplifying eq. 5.17

$$\frac{\partial \eta_E}{\partial E} = \frac{\Gamma\tau e^{\frac{2E_{min}}{\sqrt{D\tau}}} e^{\frac{-(E+Eg)}{\sqrt{D\tau}}}}{\left(e^{\frac{2E_{min}-1}{Eg}} + 1 \right) \sqrt{D\tau}} - \frac{\Gamma\tau e^{\frac{E-Eg}{\sqrt{D\tau}}}}{\left(e^{\frac{2E_{min}-1}{Eg}} + 1 \right) \sqrt{D\tau}} \quad \text{--- (5.18)}$$

From eq. 5.6 and eq. 5.18

$$J = D \frac{\frac{\Gamma \tau e^{\frac{2E_{min}}{\sqrt{D\tau}}}}{e^{\frac{-(E+Eg)}{\sqrt{D\tau}}}}}{\left(e^{\frac{2E_{min}-1}{Eg}} + 1\right) \sqrt{D\tau}} - \frac{\Gamma \tau e^{\frac{E-Eg}{\sqrt{D\tau}}}}{\left(e^{\frac{2E_{min}-1}{Eg}} + 1\right) \sqrt{D\tau}} \quad \text{--- (5.19)}$$

c = Speed of Light ($3 \times 10^{10} \text{ cmsec}^{-1}$)

d = Distance (cm)

$$c \tau = d \quad \text{--- (5.20)}$$

$$\tau = \frac{1}{\alpha c} \quad \text{--- (5.21)}$$

For 1-dimensional case

$$2Dt = \lambda^2 N \quad \text{--- (5.22)}$$

λ = Jump Distance

N = Number of Jumps = β/α

Simplifying eq. 19, eq. 20 and eq. 21

$$D = \frac{\lambda^2 \beta c}{2} \quad \text{--- (5.23)}$$

From eq. 5.21 and eq. 5.23

$$D\tau = \frac{\lambda^2 \beta}{2\alpha}$$

Or

$$\sqrt{D\tau} = \lambda \sqrt{\frac{\beta}{2\alpha}} \quad \text{--- (5.24)}$$

Modifying eq. 5.19, eq. 5.23 and eq. 5.24 and considering $E_{min} = 0$, $\lambda = 0.065 \text{ eV}$

$$\frac{-J}{\Gamma} = 0.023 \sqrt{\frac{\beta}{\alpha}} \left[e^{\frac{-(E+Eg)}{0.046 \sqrt{\frac{\beta}{\alpha}}}} - e^{\frac{(E-Eg)}{0.046 \sqrt{\frac{\beta}{\alpha}}}} \right] \quad \text{--- (5.25)}$$

Plotting $\frac{-J}{\Gamma}$ vs. E_g ,

Where, $\frac{\beta}{\alpha} = 1, 10, 100, 1000, 10,000$

$E = 0.5, 0.7, 0.9, 1.2$

$E_g=1.2$

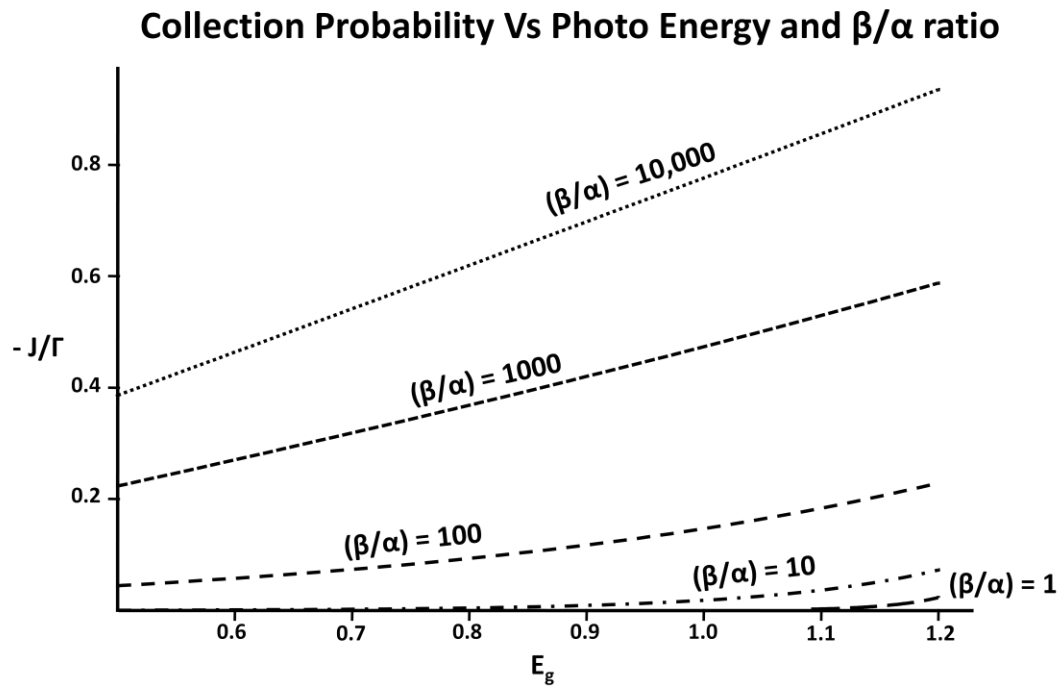


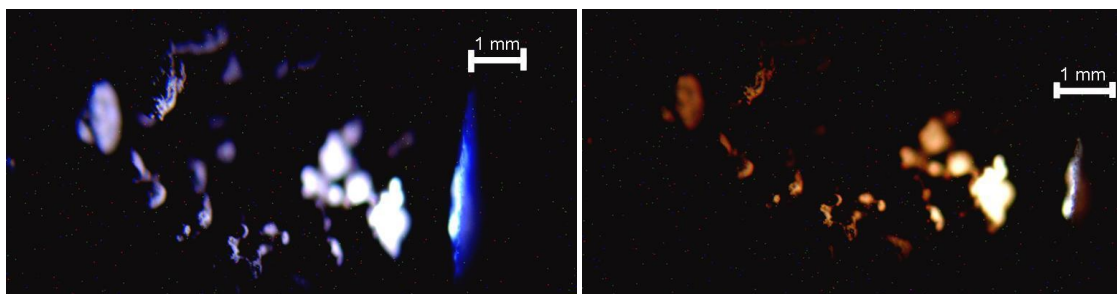
Figure 5.3: Relation between the current flux for different bandgap semiconductors.

Figure 5.3 shows the collection probability (here defined as J/Γ where J is the photon density above the bandgap value of 1.2eV and Γ is the incident photon flux – assumed here to be a constant for all energies less than the bandgap), as the probability of a Raman scattering event (β) increases relative to the probability of photon absorption (α), photons of lesser and lesser energy achieve the requisite 1.2eV energy for collection as seen.

5.3 Experiments and Results

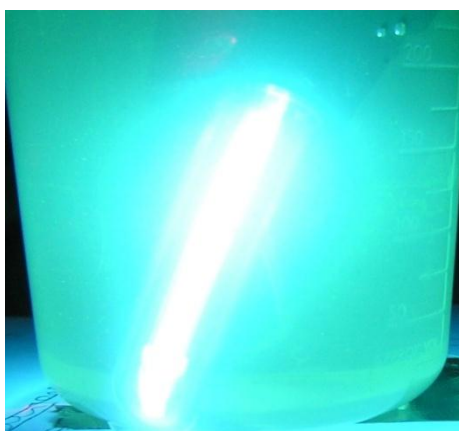
Commercially available nano-powders of 50 nm and 1 micron were obtained. In some cases the 50 nm particles were further reduced by wet chemical (HF) etching. A Thermo Nicolet Almega® micro-Raman spectrometer with a 785 nm probe beam and IR-absorption was measured using a Thermo-Nicolet FTIR. The powders were then examined under visible, UV and IR illumination both as bulk powders and suspended in solution. Powder films were applied to crystal silicon solar cells; however, the characterization of these cells is not complete at this writing.

An optical micrograph of 50 nm silicon nano particles is shown in Fig.2a. Some clumping of the nano-particles is evident. An optical micrograph of silicon nano particles under UV illumination (454 nm) in water suspension scattering a collimated laser beam (Fig.2b). Interestingly, the silicon nano particles appear to luminescence in the visible under broad spectrum (nominally 254 nm) illumination 2c.



a)

b)



c)

Figure 5.4: Optical micrographs of 50 nm silicon nano-particles under white light (a), collimated laser diode illumination (b) and broad spectrum 254 nm illumination.

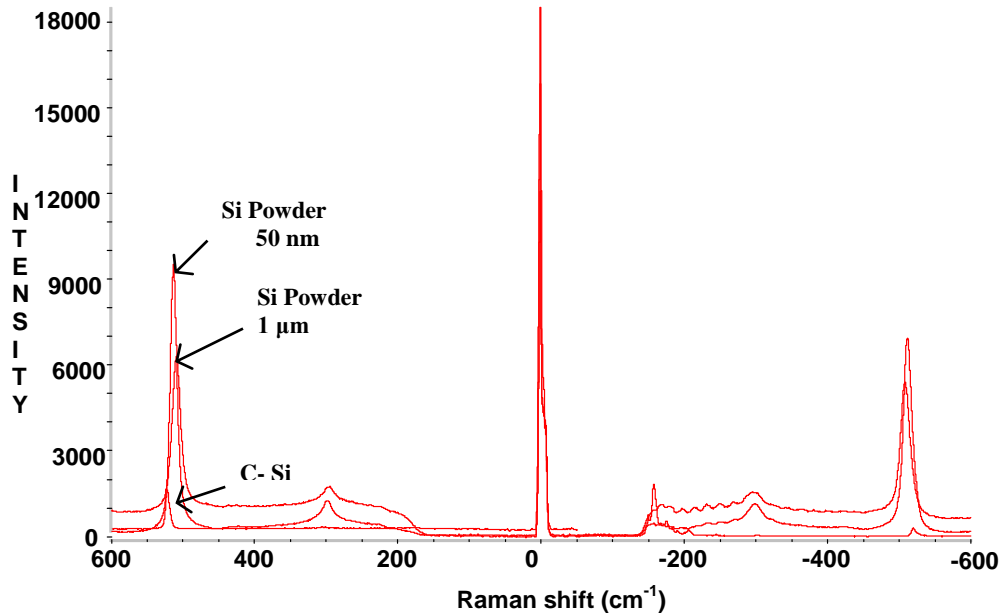


Figure 5.5: Raman shift comparison for different sizes silicon nano powder and C-silicon.

5.4 Conclusions

A theoretical and experimental study of silicon nano-particle-based spectral modification for improved solar cell performance has been initiated. Light scattering and evidence of spectral modification has been observed. Spectral down-conversion via luminescence has been observed in small ($\leq 50\text{ nm}$) silicon nano particles. Raman shift based spectral up-conversion was sought in larger $\sim 1\mu\text{m}$ silicon nano-particles. While results are encouraging more detailed experiments to determine spectral conversion efficiency are required. The potential to engineer improved amorphous silicon solar cell performance through spectral shaping coatings was explored. It is apparent that considerable gains are possible as the use of high efficiency phosphors and/or engineered materials can shift the solar spectra towards greater flux in the visible regions where the

light can be most efficiently absorbed by amorphous silicon solar cells. Embedding the spectral shifting component in a conductive, high index, large band gap media such as a-SiC:H ensures that scattered light is also introduced into the solar cell layers at large angles for increased path length and absorption increase. Thereby, thin amorphous silicon solar cells are made both more stable and more efficient. A report of the performance of commercially available phosphors and engineered up converting devices will follow.

BIBLIOGRAPHY

- [1] Haisheng Rong, Richard Jones, Ansheng Liu, Oded Cohen, Dani Hak, Alexander Fang and Mario Paniccia, "A continuous-wave Raman silicon laser," Nature 433, 725-728, 17th february 2005.
- [2] www.cornell.edu
- [3] Pavesi, L., Dal Negro, L., Mazzoleni, C., Franzo, G. and Priolo, F. Nature 408, 440-444 (2000).
- [4] Polman. A, Nature 1, 10-12 (2002).
- [5] Liu, A., Jones, R., Liao, L., Samara-Rubio, D., Rubin, D., Cohen, O., Nicolaescu, R. and Paniccia, M. Nature 427, 615-618 (2004).
- [6] Soref, R. A. Silicon-based optoelectronics. Proc. IEEE 81, 1687-1706 (1993).
- [7] A. J. Scholten, A. v. Akimov, and J. I. Dijkhuis, Phys.Rev. B47, 13, 910, (1993)
- [8] Fortmann, C.M. Phys. Rev. Lett. 81, 17, 3683, (1998)
- [9] Amorphous Semiconductors, Editor: M. H. Brodsky, Vol 36, second edition, 1985.
- [10] Chittick, R. C., Alexander, J. H., Sterling, H. F. J Electrochem. Soc. 116;77-81, 1969.
- [11] Spear, W. E. Loveland R. J. and Al-Sharbaty, A. J. Non-Cryst. Solids 15, 410 (1974)
- [12] Futako. W., Kamiya. T., Fortmann. C. M and Shimizu, I. J. of Appl. Phys., 84(3):1333-1339, 1 August, 1998.
- [13] Futako. W., Yoshino. K., Fortmann. C. M and Shimizu. I. J. of Appl. Phys., 85(2):812-818, 15 jan. 1999.
- [14] Fukutani, K., Kanbe, M., Futako, W., Kaplan, B., Kamiya, T., Fortmann, C. M and Shimizu, I, J. Non-Crystalline Solids, 227-230:63-67, 1998.
- [15] Manfredotti, F., Fizzotti, F., Boero, M., Pastorino, P., Vittone, E and Rigato, V. Mat. Res. Soc. Symp. Proc., Vol 297, 231-236, 1993.
- [16] Kessels, W. M. M., Severns, R. J., Van De Sanden, M. C. M and Schram, D.C. J. Non-Crystalline Solids, 227-230:133-137, 1998.

- [17] Nabil M. Amer and Warren Jackson. Optical properties on defect states in a-Si:H. In J. Pankove, editor, Semiconductors and Semimetals, Vol 21 Part B, Chapter 3, 83-112, Academic Press, New York, 1984.
- [18] Zanzucchi, P. J., Wronski, C. R., Carlson, D. E. J. Appl. Phys. 48:5227-36, 1977.
- [19] Joannopoulos, J. D., Cohen, M. L. Solid State Physics. 31:71-148, 1976.
- [20] Beyer, W, "Hydrogen Phenomena in Hydrogenated Amorphous Silicon" Chp 5, Semiconductors and Semimetals. 61. Academic Press, NY, 165-239, 1999.
- [21] Fortmann, C. M., Jaen, E. L., Proceedings of SPIE, Vol.3801, 24-35. 1999.
- [22] Fortmann, C. M., Jaen, E. L., Hata, N. Proceedings SPIE, Vol 4110, 195-203. 200.
- [23] Fortmann, C. M., Luryi, S., Tonucci, R., Coleman, J. H., US Patent 6,064,511, issued May 16 2000.
- [24] Fortmann, C. M., Jaen, E. L., Hata, N., Anderson, W. A and Mahan, A. H. Thin Solid Films.395, 142-146. 2001.
- [25] Nelson, B. P., Xu, Y., Mahan, A. H., Williamson, D. L and Crandall, R. S. Mat. Res. Soc. Symp. Proc. 609, A22.8.1-A22.8.6, San Francisco, CA 2000.
- [26] Fortmann, C. M., Mahan, A. H., Ward, S., Anderson, W. A., Tonucci, R and Hata, N. Thin Solid Films. 430, 278-82. 2003.
- [27] Fortmann, C. M., Jaen, E. L., Anderson, W. A., Mahan, A. H and Hata, N. SPIE. Proc. 4459, San Diego, CA, 10-19. 2001.
- [28] Rong, H., Jones, R., Liu, A., Cohen, O., Hak, D., Fang A., Paniccia, M. Nature. 433, 725-727, 2005.
- [29] Kittel, C. "Introduction to Solid State Physics" Chp 11, John Wiley and sons, Inc., New York.
- [30] Scholten, A. J., Dijkhuis, J. I. Phys. Rev. Lett. 53, 7, 3836-3840, 1996.
- [31] Scholten, A. J., Akimov, A. V., and Dijkhuis, J. I. Phys. Rev. Lett. 47, 20, 910-913, 1993.
- [32] Scholten, A. J., Akimov, A. V., and Dijkhuis, J. I. Phys. Rev. Lett. 54, 17, 151-161, 1996.
- [33] Wakagi, M., Ogata, K., and Nakano, A. Phys. Rev. Let. 50, 15, 666-671, 1984.

- [34] Zeghbroek, V. B. "Principles of Semiconductors Devices" Chp 4, <http://ece-www.colorado.edu/bart/book.htm>.
- [35] Joannopoulos, J. D., Meade, R. D and Winn, J. N., "Photonic crystals, modelling the flow of light," Pinceton University Press, Princeton, NJ. 1995.
- [36] Soukoulis, C. M."Photonic bandgaps and localisations," NATO ASI. ser. B.Vol. 308.
- [37] Yablonovitch, E. Phys. Rev. Let. 58, 2059 (1987).
- [38] Fortmann, C. M. "Non-Crystalline materials for optoelectronics". Edited by Lucovsky, G., Popeslu, M. Vol 1, Chp 14.
- [39] Hata N., Fortmann, C. M., Matsuda, A. Mat. Res. Soc. Symp. Proc. Vol 664. Materials Research Society. 2001.
- [40] Yablonovitch, E., Photonic Band Gaps and localization, NATO, ASI, Ser. B, Vol. 308 (plenum Press, New York, 1993).
- [41] Photovoltaic Materials, Richard H. Bube., Series on Properties of Semiconductor Materials – Vol 1. 1998.
- [42] www.easthorse.net
- [43] <http://www1.eere.energy.gov>
- [44] www.pvcdrom.pveducation.org
- [45] Nelson. B.P, Atwater, H.A., von Roedern, B., Yang, J., Sims, P. Deng, X., Dalal, V., Carlson, D., Wang, T., "Amorphous and Thin-Film Silicon", NREL, 2003.
- [46] N. Bernhard, G.H. Bauer and W.H. Bloss, Band Gap Engineering of Amorphous Semiconductors for Solar Cell Applications, Progress in Photovoltaics **3**, 149 (1995).
- [47] J. Yang, R. Mohr, R. Ross, Technical Digest of the International PVSEC-1, Kose, Japan, A-II6-L6, 1984.
- [48] Z. Smith, S. Alijishi, V. Chu, J. Conde, and S. Wagner, Tech. Digest 3rd Photovoltaic Sci. Eng. Conf., Tokyo (1987).
- [49] G. B. Turner, R. J. Schwartz, J. L. Gray and J. W. Park, 19th IEEE photovoltaic specialists conference, New Orleans, IEEE publishing, NY (1987).
- [50] J. Yang, B. Yan, S. Guha, Thin Solid Films, 487 (2005).
- [51] J. Yang, A. Banerjee, S. Guha, Solar Energy Materials & Solar cells, 78 (2003).

- [52] L. T. Canham, *Appl. Phys. Lett.* 57, 1046 (1990).
- [53] Liu. S., *Journal of Nanoscience and Nanotechnology*, 8, 1110 (2008).
- [54] L. Paveshi, L. D. Negro, C. Mazzoleni, G. Franzo, and F. Priolo, *Nature (London)* 408, 440 (2000).
- [55] S. Coe, W. Woo, M. Bawendi, and V. Bulovic, *Nature (London)* 420, 800 (2002).
- [56] T. Tsutsui, *Nature (London)* 420, 752 (2002).
- [57] W. U. Huynh, J. J. Dittmet, and A. P. Alivisatos, *Science* 295, 2425 (2002).
- [58] I. Matsui, *J. Chem. Eng, Jpn.* 38, 535 (2005).
- [59] B. Sun, E. Marx, and N. C. Greenham, *Nano Lett.* 3, 961 (2003).
- [60] K. A. Littau, P. J. Szajowski, A. J. Muller, A. R. Kortan, and L. E. Brus, *J. Phys. Chem.* 97, 1224 (1993).
- [61] L. E. Brus, P. J. Szajowski, W. L. Wilson, T. D. Harris, S. Schuppler, and P. H. Citrin, *J. Am. Chem. Soc.* 117, 2915 (1995).
- [62] H. Takagi, H. Ogawa, Y. Yamazaki, A. Ishizaki, and T. Nakagiri, *Appl. Phys. Lett.* 56, 2379 (1990).
- [63] M. Yamamoto, K. Hayashi, K. Tsunetomo, K. Khono, and Y. Saka, *Jpn. J. Appl. Phys. Part 1* 30, 136 (1991).
- [64] Y. Osaka, K. Tsunetomo, F. Toyomura, H. Myoren, and K. Khono, *Jpn. J. Appl. Phys. Part 2* 31, L565 (1992).
- [65] C. W. White, S. P. Withrow, A. Meldrum, J. D. Budai, D. M. Hembree, J. G. Zhu, D. O. Henderson, and S. Praver, *J. Appl. Phys.* 78, 4386 (1995).
- [66] Borsella, M. Falconeri, S. Botti, S. Martelli, F. Bignoli, L. Costa, S. Grandi, L. Sangaletti, S. Allieri, and L. Depero, *Mater. Sci. Eng. B* 79, 55 (2000).
- [67] S. Botti, R. Coppola, F. Gourbilleau, and R. Rizk, *J. Appl. Phys.* 88, 3396 (2000).
- [68] X. Li, Y. He, S. S. Talukdar, and M. T. Swihart, *Langmuir*, 19, 8490 (2003).
- [69] X. Li, Y. He, S. S. Talukdar, and M. T. Swihart, *Phase Transitions: A Multinational Journal*, 77, 131 (2004).
- [70] X. Li, Y. He, and M. T. Swihart, *Langmuir*, 20, 4720 (2004).

- [71] G. Belomoin, J. Therrien, A. Smith, S. Rao, R. Twesten, S. Chaieb, M. H. Nayfeh, L. Wagner, and L. Mitas, *Appl. Phys. Lett.* 80, 841 (2002).
- [72] A. D. Yoffe, *Adv. Phys.* 50, 1 (2001).
- [73] W. L. Wilson, P. F. Szajowski, and L. E. Brus, *Science* 262, 1242 (1993).
- [74] A. P. Alvisatos, *Mater. Res. Bull.*, 19, 23 (1995).
- [75] H. Heckler, D. Kovalev, G. Polisski, N. N. Zinov'ev, and F. Koch, *Phys. Rev. B* 60, 7718 (1999).
- [76] M. V. Wolkin, J. Jorne, P. M. Fauchet, G. Allan, and C. Delerue, *Phys. Rev. Lett.* 82, 197 (1999).
- [77] J. P. Wilcoxon, G. A. Samara and P. N. Provencio, *Phys. Rev. B* 60, 4, 2704 (1999).
- [78] D. Kovalev, H. Heckler, B. Averboukh, M. Ben-chorin, M. schwartzkopff, and F. Koch, *Phys. Rev. B* 57, 3741 (1998).
- [79] Schuppler, S. L. Friedman, M. A. Marcus, D. L. Adler, Y. H. Xie, F. M. Moss, Y. L. Cha-bal, T. D. Harris, L. E. Brus, W. L. Brown, E. E. Chaban, P. F. Szajowski, S. B. Christman, and P. H. Citrin, *Phys. Rev. Lett.* 72, 2648 (1994); *Phys. Rev. B* 52, 4910 (1995).
- [80] S. Ossicini, L. Pavesi, F. Priolo, *Light emitting silicon for microphotinics*, Springer Tracts in Modern Physics Vol 194. Springer-Verlag: Berlin, 2003.
- [81] H. Rong, et al., *Nature*, 433, 725, (2005).
- [82] *Appl. Phys. Lett.* 70 (6), (1997).
- [83] C. M. Fortmann, *Phys. Rev. Lett.* 81, 17, 3683, (1998).
- [84] J. A. Mawyin, S. G. Chawda, R. J. Gambino, C. R. Clayton, R.J. Tonucci, C. M. Fortmann, *Mat. Res. Soc.* Submitted, 2008.
- [85] J. D. Jackson, *classical Electrodynamics*, 3rd edition, Wiley, 1999.
- [86] K. Winz, C.M. Fortmann, Th. Eichkoff, C. Beneking, H. Wagner; and, H. Fujiwara and I. Shimizu, *Solar Energy Materials and Solar Cells* 49, 195, (1997).
- [87] Carlson, *Semiconductor and Semimetals*, Vol. 21, Hydrogenated Amorphous Silicon Part D, J. Pankove ed., Academic, 1984.

[88] J. A. Mawyin, S. G. Chawda, G. P. Halada, C. R. Clayton, C. M. Fortmann, "Substrate Engineering for High Efficiency Thin Film Solar Cells", *Journal of Non-crystalline Solids* 354, 2492-2494, (2008).

[89] A. Shalav, B.S. Richards, M.A. Green, *Solar Energy Materials & Solar Cells* 91, 829, (2007).